TURUN
YLIOPISTO
Matemaattis-luonnontieteellinen
tiedekunta

Optimization of photochromic Br-hackmanite materials for optical film and eyewear applications

Bettiina Muurinen

Master's thesis

Intelligent materials chemistry

University of Turku

Department of Chemistry

October 2024

Master's thesis

Subject: Chemistry
Author: Bettiina Muurinen
Title: Optimization of photochromic Br-hackmanite composites for optical film and eyewear applications
Supervisors: Mika Lastusaari, Hannah Byron, Sami Vuori
Number of pages: 44 p.
Date: October 2024

Hackmanite ($Na_8(Al_6Si_6O_{24})(Cl,S)_2$), a sulfur-doped sodalite mineral, exhibits reversible photochromism, meaning it changes color under UV light and fades back to its initial color when exposed to visible light or heat. This unique property makes hackmanite a promising candidate for applications in photochromic eyewear, optical coatings, and UV sensors. As the amount of harmful UV radiation reaching the Earth's surface has significantly increased in recent years, there is a growing need for effective UV protection and monitoring tools. Photochromic sensors that change color under UV light provide a rapid, visual indication of excessive UV exposure. Similarly, photochromic eyewear darkens in sunlight, functioning like sunglasses to protect the eyes and the sensitive surrounding skin from harmful radiation.

In this work, the primary goal was to determine optimal synthesis conditions for hackmanite, enhance its photochromic response, and evaluate its suitability for photochromic films and potential eyewear applications. Bromide was substituted for chloride in the hackmanite structure, and various parameters, including annealing and reduction temperatures, grinding duration, and boron addition, were investigated to enhance the material's photochromic properties. Hackmanite films were fabricated with attention to mass percentage optimization, thickness consistency, and aggregation control through surfactants. The results showed that higher color intensity resulted in more opaque material, and that attempts to enhance transmittance through aggregation control or reducing the crystallite size were ineffective. These limitations suggest that there are significant challenges hindering the development of a transparent hackmanite lens material suitable for commercial use, and further research needs to be done. However, while hackmanite may not be ideal for transparent applications like eyewear, it holds significant potential for UV sensors and similar applications where transparency is not a critical requirement.

Key words: hackmanite, photochromic eyewear, UV sensoring, photochromism

Table of contents

Abbreviations

UV radiation – ultraviolet radiation

m-% – mass percentage

XRD – X-ray diffraction

XRF – X-ray fluorescence

SEM – scanning electron microscopy

1. Introduction

1.1. Reversible photochromism

Intelligent materials, also called smart materials, are advanced substances that can reversibly change their properties in response to external stimuli, such as light, temperature, pH, or electrical fields. Among these, photochromic materials stand out for their ability to reversibly change color upon exposure to light. The color change of such materials is typically induced by UV light, and the color returns to its original, uncolored state through heating or exposure to visible light.[1] This unique feature called photochromism, or tenebrescence, is especially promising in applications such as UV indexing[2,3], optical information storage[4], energy-saving window glass[5], X-ray imaging[6], optical switches[7], and photochromic eyewear[8–10]. With the increasing interest in photochromic materials, there is a growing demand for cheaper, more durable, and environmentally friendly alternatives. Hackmanite, a sodalite mineral, is one such material showing promising properties due to its modifiability and abundance of natural sodalite.[11] The following sections will explore the unique role of hackmanite among photochromic materials, highlighting its potential to overcome the limitations of conventional organic and inorganic compounds through its defect-induced photochromic mechanism.

The reversible color change in photochromic materials occurs due to a chemical transformation, where absorption under specific wavelengths of electromagnetic radiation differs significantly between the two forms.[12,13] This reversible transformation often involves structural or conformational changes, which may also lead to additional changes in the materials properties beyond just the absorption. These changes may include shifts in refractive index[14], fluorescence[15–17], electrical conductivity[18], and opacity[19], for example.

Photochromic materials that change color under UV radiation include inorganic, organic, and hybrid compounds. Well-known organic photochromic compounds include spiropyran[20–22], spirooxazine[21], azobenzene[23]. These compounds typically contain a conjugated π-system, which enables large resonance. These structural features enable unimolecular reactions, such as cis-trans isomerizations, ring closing and opening, and intramolecular proton transfers, which are plausible for their photochromic behavior.[20–23]

Organic photochromic molecules have high photosensitivity, but they often suffer from degradation of switching efficiency, as they cannot withstand many color-changing cycles. In addition to the rapid deterioration of photochromism, organic compounds are challenged by steric hindrances in their structures and low photostability. Especially the weak heat and long-term light stability of organic photochromic systems limit the potential applications.[1,21] Inorganic materials,

such as tungsten oxide (WO_3) and molybdenum trioxide (MoO_3) offer several advantages, including thermal stability, mechanical strength, and much better fatigue resistance. However, they typically exhibit much lower photochromic contrast and pose environmental concerns due to the presence of heavy metals. These compounds are also relatively expensive, which limits their practical applicability.[24,25] The photochromic behavior in inorganic materials can generally be explained with two mechanisms: the color change is attributed to photon-induced electron-hole pairs that are trapped by defects within the material, or the hopping of valence electrons that generate charge transfer.[26] While inorganic photochromic materials do not have such vast range of colors as organic ones, their durability, mechanical strength, and temperature resistance are much better, and they are also much easier to produce.[25,26]

While organic photochromic materials suffer from degradation and inorganic compounds are often environmentally concerning, photochromic sodalite, also called hackmanite, presents a promising alternative. This unique, intelligent mineral with the general formula $Na_8(Al_6Si_6O_{24})(Cl,S)_2$ is particularly interesting due to its tunability, as well as its cost-effective and simple synthesis. Its defect-based photochromic mechanism allows for virtually endless color-changing cycles without compromising structural integrity, addressing some of the challenges common with traditional photochromic materials. Although hackmanite is a naturally occurring mineral, it can also be synthesized via several methods, including solid-state reactions or hydrothermal synthesis. Hackmanite's composition has been successfully modified in several research studies[4,27–31], suggesting that its properties could be further enhanced through continued research.

1.2. Photochromic sodalites

Sodalite ($Na_8Al_6Si_6O_{24}Cl_2$), discovered in 1806 by Karl Ludvig von Giesecke (1761–1833), is the sodium-rich member of the sodalite mineral group. Sodalite minerals have a general formula of $M_8(T'T''O_4)_6X_2$, where the M-site typically consist of mono- or divalent elements such as Ca, K, Li, Na, Sr, or Mn. The T-site consists of tetrahedrally coordinated elements, including Al, Si, B, and Be. The X-side varies widely, and it can include anions like Cl^-, Br^-, S^-, I^-, or molecules such as SO_4^{2-}, CO_3^{2-} or OH^-, for example.[32]

The framework of sodalite is composed of ordered SiO_4 and AlO_4 tetrahedra, which create so called β-cages within the structure. Each β-cage contains a large Cl^- anion, which is tetrahedrally coordinated by four Na^+ cations. Chemical impurities, vacancies and structural defects within the sodalite framework can significantly influence its properties. A particularly notable example is the mineral hackmanite, in which the Cl^- ion is partially replaced by a S_2^{2-} ion. This substitution generates a chloride vacancy (V_{Cl}) in the β-cage structure to maintain charge neutrality **(Figure 1)**.[1,12,32] This inclusion of sulfide and vacancy results in small enlargement of the structure[1]. These structural

features, along with the easy doping, enable hackmanite to exhibit reversible photochromism[1,12,31,32], persistent luminescence (PeL)[28,33], thermoluminescence[30], and photoluminescence[34].

Hackmanite is therefore a sulfur-doped sodalite mineral, and although the correct nomenclature, according to the International Mineralogical Association is photochromic sodalite,[35] the term hackmanite will be used in this study, as it is widely established in the published research. Hackmanite exhibits a photochromic color change when exposed to UV, X-ray, or gamma radiation, returning back to its original state under visible light or heat.[6] This color change, unlike in organic color-changing compounds, can occur practically indefinitely without degradation. This, together with the easy and cheap synthesis of hackmanite have led to growing interest in its potential applications, including detection and measurement of UV- and gamma radiation, and diagnostics.[3,4,6,36]

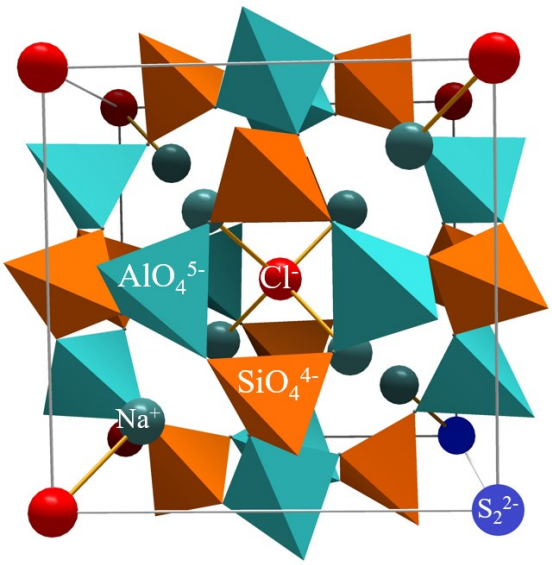

Figure 1. *Hackmanite unit cell, consisting of SiO_4 and AlO_4 tetrahedra, and Cl^-, Na^+ and S_2^{2-} ions in the sodalite cage. In natural hackmanite the anion is chloride, but in this study, it was replaced by bromide. The figure is modified from a research article written by Vuori et al.[4]*

1.2.1. Hackmanite's photochromism

Under UV light, hackmanite changes color from white to pink or purple, and the color then fades to the white shade under visible light. The color change is initiated when UV radiation excites the valence electron of the anionic disulfide ion (S_2^{2-}), causing the electron to move to a nearby chloride vacancy (V_{Cl}) within the sodalite framework. The vacancy stabilizes the negative charge of the sulfide, maintaining charge neutrality in the structure. The chemical equation for this mechanism is shown below.

$$S_2^{2-} + V_{Cl} \rightleftharpoons S_2^- + V_{Cl}^- .$$

This process creates an F-center at the anionic vacancies, altering the optical properties of sodalite by enabling it to absorb visible light. This radiation, together with the excitation energy of the electron, causes the purple color. When enough energy is applied, such as visible light or heat, electrons are released from the F-center and return to the disulfide anion, causing the purple color to fade away. This means that when there is not enough light or heat present, the F-centers can last permanently.[1,6,32,34]

The lattice parameter increases, albeit only by a small amount, when F-centers are formed, and hackmanite is in the colored form. The framework geometry remains the same, but the bond distances and ion positions undergo some small changes. This is due to the redistribution of electrons in the framework, as they transfer from the sulfide to the vacancy.[1,12] The interaction between sodium and the F-center structure with an electron and S_2^- is stronger compared to the bleached form, where the vacancies are not filled. This electrostatic interaction pulls sodium more towards the trapped electron and thus increases the Na–O distance. The impact of this electron transfer varies within the whole structure, as the majority of the sodium ions are located near cages that have chloride ions instead of the vacancies, and thus do not take part in the photochromic mechanism.[1] This work is focused on hackmanite where chloride is replaced with bromide. This is done to expand the unit cell, and that way decrease the excitation energy, as this change allows the hackmanite to absorb light at longer wavelengths.[31]

The depth of the color depends on factors such as the wavelength and intensity of excitation, crystallite size of the hackmanite, and the size and density of the F-centers[1,33]. The color change can occur practically indefinitely, as no chemical bonds are broken in the process, and the hackmanite's sodalite cage structure remains intact, as the F-center forms in the pores of it.[12]

1.3. Photochromic glasses and films

The skin around the human eye is very delicate and prone to sunburn and skin cancer, and even minimal levels of UV radiation can cause damage to the eye.[37] Atmosphere blocks out the most harmful, highest energy UV-C radiation, but much of UV-A and UV-B radiation reach the Earth surface. Thus, it is very important to correctly protect the eyes from the harmful UV radiation from the sun. Photochromic eyeglasses, which protect the eye by darkening like sunglasses when exposed to UV radiation outdoors, offer a promising solution for UV protection. When returning indoors, the color fades away in the presence of visible light and no UV light. By blocking UV radiation, photochromic lenses also reduce eye strain and eye damage. Compared to sunglasses, photochromic lenses are convenient because they function as both eyeglasses and sunglasses, making them easier to use. Especially if one must use glasses also indoors, using photochromic eyeglasses removes the need for changing from sunglasses to normal eyeglasses when returning indoors.[38,39]

Photochromic sunglasses protect the eyes from harmful UV radiation, but UV sensors monitor the UV exposure, telling when to protect better from the sun. This monitoring is increasing its importance, as nowadays the awareness of the harmful side effects of UV radiation is increased. Photochromic UV sensors show a visible color change when exposed to UV light, offering an instant and easy way to detect harmful UV radiation.[2,3,40]

In addition to films and lenses, photochromic glass windows have gained significant attention recently due to their potential to reduce energy losses associated with inefficient window systems, which often allow excessive heat transfer in and out of buildings. Buildings account for the largest part of global energy consumption, responsible for 30–40% of the total energy used globally, with windows contributing significantly to this inefficiency.[5,41,42] Especially in regions with hot climate and intensive sunlight, the demand for air conditioning is particularly high. Photochromic windows reduce the transmission of light through the window in bright conditions, thus reducing the reliance on air conditioning. Furthermore, on cloudy days the windows remain transparent, allowing natural light to transmit through without the need for additional window coverings, making them a practical and energy-sufficient solution.[5]

In the field of photochromic ophthalmic lenses, silver halides – particularly silver chloride, and often silver bromide – were among the most widely used materials.[8,21] Photochromic silver halide glass was first successfully manufactured in 1964 by Armistead and Stookey.[9] The photochromic mechanism in silver halides is based on ionic valence changes within the glass matrix.[26] When irradiating the glass with UV light, electrons are excited from chloride ions, forming chlorine atoms. These electrons reduce silver ions to silver atoms, which absorb visible light and cause coloration. In visible light the process reverses, and the color fades. This reversible process is maintained by the glass matrix, which traps the halogen atoms near silver ions, also preventing unwanted side reactions due to its hydrophobic, inert, and rigid nature.[8,9,43]

Silver halide-based glass lenses were popular primarily in the earlier generations of photochromic eyewear. Today, plastic lenses based on organic dyes dominate the market since John Crano's breakthrough with these materials in the mid-1980s. Crano developed photochromic lenses using naphthoxazines and naphthopyrans, which were commercialized under the Transitions™ brand.[44,45] Glass lenses using silver halides are heavier and more fragile, while organic dyes are embedded in plastic lenses, making them lighter and more impact-resistant. Most modern photochromic lenses are based on polycarbonate polymers and naphtopyran-based organic dyes. These include the latest Transitions™ lenses, as well as Hoya Sensity™, Drivewear®, Photofusion®, and Essilor® lenses.[46–50]

Producing photochromic lenses with heavy metals can be costly and may involve environmentally harmful processing steps, while organic compounds, even though having smaller environmental impact, are typically less durable. Therefore, this work explored the use of hackmanite in photochromic lenses, as hackmanite is both easy and cheap to produce, environmentally friendly, and can change color virtually indefinitely. Moreover, defects-induced photochromism, that hackmanite is also based on, has not been studied nearly as much as the other types of mechanisms and materials based on them. This rises the importance of the research concerning hackmanite, as the tunability of it may give crucial possibilities in the field of photochromic lenses and films.

1.4. The background and goal of this work

The primary aim of this work was to produce color-changing photochromic films using hackmanite, due to its excellent properties, and then to explore the synthesis of hackmanite-infused glasses. The project initially focused on synthesizing hackmanite with characteristics that include rapid coloration, a low excitation threshold, and a deep color. Hackmanite films were prepared by combining hackmanite with silicone elastomer, with the hackmanite mass percentage optimized to prevent cloudiness while still achieving a sufficiently deep color. Production parameters were further refined to ensure high absorptance and small crystalline size, enhancing the films' overall optical performance.

Additionally, several essential properties of hackmanite films, such as coloration rate, fading rate, transmittance, appearance, and thickness, were evaluated. This evaluation was done to determine hackmanite's suitability for use in photochromic films or lenses, and to identify any material adjustments needed for optimal performance.

Although the project initially aimed to synthesize hackmanite-infused glasses, simultaneous unpublished research within the same research group suggested that incorporating hackmanite into a glass matrix did not yield promising results. Based on these findings, the synthesis of hackmanite glasses was not pursued further in this study. Instead, the focus remained on optimizing the synthesis of hackmanite films and collecting critical data to support future research in this area. By focusing on hackmanite films, this work aims to lay the groundwork for potential applications in photochromic lenses, UV sensors, and energy-efficient windows, where hackmanite's properties could offer distinct advantages.

2. Experimental

Hackmanite was synthesized using two different methods: solid-state and precipitation. Various experimental parameters were investigated to optimize the synthesis process, including annealing and reduction temperatures, the duration of these processes, and the techniques used for reduction. Additionally, the influence of various precursor additives was examined to evaluate their impact on

the synthesis efficiency and the resulting properties of hackmanite. The following sections outline the specific procedures and experimental conditions used in each synthesis method, as well as the modifications made to evaluate hackmanite's structural, optical, and photochromic characteristics.

2.1. Solid-state synthesis

Multiple batches of hackmanite were synthesized using the solid-state synthesis method, following the synthesis route detailed in Chapter 2.1.1. below. While the general synthesis route remained consistent, certain variations were introduced in specific batches, which are detailed in their respective sections. Additionally, depending on the temperature, number of samples, and overall availability, the type of furnace used for syntheses differed among batches. The furnace models used for each sample are listed in **Table S1** in Supporting Information. It is important to note that variations in furnace models may influence thermal profiles and subsequently affect the properties of the synthesized hackmanite, as each furnace may have unique thermal characteristics.

2.1.1. The grinding set

The grinding set samples were prepared to optimize the grinding process, with the goal of achieving a small crystallite size. Smaller crystals are essential for preventing the formation of fuzzy hackmanite films, as larger crystals may contribute to uneven film surfaces and enhanced aggregation. The starting materials used in solid-state synthesis were zeolite A (Sigma–Aldrich), sodium sulfate (Na_2SO_4, Sigma–Aldrich, ≥ 99 %), and sodium bromide (NaBr, J.T.Baker, ≥ 99 %). Before use, all materials were dried in air at 500 °C for one hour in a Nabertherm N3/C8 furnace to remove any residual moisture.

For each sample, 1.667 g of zeolite A, 0.10 g of Na_2SO_4, and 0.69 g of NaBr were weighed using a plastic spoon and paper to minimize metal contamination. Six of these mixtures were then ground and homogenized in an agate mortar for 5 minutes, and then transferred to alumina crucibles for the initial heating. For this annealing part, the heating temperature was set to 850 °C, heating rate to 3 °C/min and dwelling time to 5 hours.

After the initial heat treatment, the samples were ground again in an agate mortar for 5 minutes to ensure uniformity. The samples were then transferred back into alumina crucibles and placed back into the furnace for reduction. A reducing atmosphere was created using Formier gas (10 % hydrogen and 90 % nitrogen), and the reduction was conducted at 850 °C with a heating rate of 18 °C/min for 2 hours. Once the furnace had cooled down freely below 100 °C, the gas supply was turned off, and the crucibles were removed from the furnace once the temperature had decreased to below 60 °C.

After reduction, the hackmanite samples were further ground in an agate mortar for 5 minutes, after which they were washed with water three times using Heraeus Biofuge Stratos centrifuge operating

at 1400 rpm for 5 minutes per cycle, to remove any residual impurities. The washed samples were dried overnight at 80 °C in an incubator. To examine the effect of grinding techniques on crystal size, the dried samples underwent two types of grinding. One sample was manually ground in an agate mortar for 5 minutes, while the remaining five samples were ground using a ball mill at a constant speed setting of 5 (corresponding to 1730 rpm motor speed). Each of these five samples was ground for varying durations of 2.5, 5.0, 7.5, 10.0, or 12.5 minutes, with each interval differing by 2.5 minutes. For consistency, the samples are designated as H0, H2.5, H5, H7.5, H10, and H12.5, corresponding to their respective grinding times in the ball mill.

2.1.2. Addition of boron

The addition of boron was investigated to explore whether it could produce a glassy material by modifying the solid-state synthesis route established by R. Radler[51]. Radler's research focused on creating glass-like sodalite materials through the incorporation of flux agents, such as boric oxide (B_2O_3). He found that certain samples, most notably sample he referred as H-11-S-3, exhibited excellent tenebrescent properties in a glassy, translucent form. This particular sample used "H-11" as one of the starting materials, which was synthesized by firing a mix of Na_2CO_3, Al_2O_3, and silicic acid at 900 °C in three cycles.

In the modified synthesis, Zeolite A and NaBr were substituted for H-11 and NaCl, respectively. Initially, only the addition of boron was pursued to test its effects on the product, following the same procedure as the standard solid-state method outlined previously. The starting material quantities were kept consistent with Radler's work, using 1.8 g of Zeolite A, 0.067 g of Na_2SO_4, 0.2817 g of NaBr and 0.1 g of B_2O_3 (Merck, ≥ 99 %). To assess the impact of boron concentration, an additional sample containing only 0.05 g of B_2O_3 was prepared. Both samples were ground in an agate mortar, then placed into alumina crucibles, and same annealing and reduction protocols as detailed in Chapter 2.2.1. were conducted. After reduction, the samples were washed three times with water, dried overnight at 80 °C, and then ground in a ball mill for 7.5 minutes at speed 1400 rpm.

After obtaining good results with the addition of boron, the syntheses conducted by Radler were further explored. In addition to the previously mentioned H-11-S-3, also synthesis of Radler's sample H-76-11 was investigated to examine the effects of substituting boric acid (H_3BO_4) for boric oxide (B_2O_3). The sample H-76-11 was selected to determine whether this substitution would lead to any notable differences in the material's properties.

To begin, a new batch of hackmanite, excluding boron, was synthesized following the procedure detailed in Chapter 2.2.1. The synthesis involved six samples, each composed of 1.667 g of Zeolite

A, 0.10 g of Na_2SO_4, and 0.69 g of NaBr, which were ground for 5 minutes and placed in alumina crucibles for the established annealing, reduction, and grinding steps.

For the synthesis of sample H-76-11, 0.9804 g of the previously synthesized hackmanite, 0.0490 g of H_3BO_4 (Merck ≥ 99.8 %), and 0.1381 g of NaBr were combined. Similarly, H-11-S-3 was synthesized with 1.8 g of Zeolite A, 0.067 g of Na_2SO_4, 0.2817 g of NaBr, and 0.1 g of B_2O_3. Both samples were then ground for 5 minutes and transferred to alumina crucibles for the reduction process, following Radler's conditions. No separate annealing was performed. The samples were reduced in a Formier gas atmosphere (10 % H_2 / 90 % N_2) at 1100 °C, with a heating rate of 10 °C/min and a dwelling time of 30 minutes. After reduction, the samples were ground in an agate mortar, washed three times with distilled water, and dried overnight at 80 °C.

To further assess the effect of higher boron content, additional hackmanite samples with higher boron amount of 0.14 g and 0.17 g were synthesized. These samples were prepared following the same procedures as the two initial boron-doped samples, including both annealing and reduction. However, as these samples did not exhibit good results, the experiments with boron were not conducted further. For consistency, the samples with added boron are designated as BH0.05, BH0.1, BH0.14, and BH0.17, corresponding to the calculated B_2O_3 mass percentage. Samples H-76-11 and H-11-S-3 are designated as in the original study by R. Radler[51].

2.2. Precipitation from an aluminosilicate solution

Hackmanite was also synthesized by precipitation from an aqueous aluminosilicate solution, with the goal of obtaining smaller particles. This synthesis method was adapted from procedures developed by Hund et al.[52] The detailed synthesis procedure is outlined as follows:

1. Preparation of sodium hydroxide solution: 63 g of NaOH (J.T.Baker, ≥ 98 %) was weighed and dissolved in 77 g of crushed ice in an Erlenmeyer flask. The mixture was stirred rapidly, as the reaction is exothermic, and NaOH tends to adhere to glass surfaces. The use of ice reduces the heat generated during dissolution.
2. Addition of aluminum: Once the sodium hydroxide was fully dissolved, 1.08 g of aluminum (Sigma–Aldrich, ≥ 99 %) was carefully added to the mixture, while continuously stirring with a magnetic stirrer. The aluminum then dissolves in the basic solution, generating aluminum ions necessary for the aluminosilicate framework.
3. Addition of salts: After complete dissolution of the aluminum, 20.876 g of NaBr and 3.0255 g of Na_2SO_4 were added to the solution. These salts serve as the precursors for bromide and sulfate ions.
4. Filtration: The mixture was then transferred to a vacuum flask and filtered to remove any excess aluminum.

5. Addition of sodium silicate: The filtered solution was transferred to a round-bottom flask, and 10 ml of sodium silicate (Sigma–Aldrich) was added via a dropping funnel while continuously stirring. The silicate ions complete the aluminosilicate framework of hackmanite.
6. Reflux: The solution was refluxed for 24 hours at 105 °C. After refluxing, the resulting white crystalline product was filtered, washed thoroughly with distilled water, and dried overnight at 80 °C in an incubator.
7. Reduction: The dried product was reduced in a furnace under a reducing H_2/N_2 atmosphere at 850 °C for 2 hours, following the same reduction procedure used in the solid-state synthesis method. Once the reduction was complete, the hackmanite was ground in a ball mill for 7.5 minutes in speed 5 to achieve a uniform particle size

2.2.1. Reduction tests

In previous experiments, hackmanite was reduced in a furnace at 850 °C using a reducing Formier gas atmosphere, as outlined in earlier sections. Given that the precipitation method may act as an alternative to the initial annealing step in solid-state synthesis, an alternative reduction method was tested to determine whether hackmanite could be reduced without the need for a furnace. This alternative approach involved using sodium borohydride ($NaBH_4$, Sigma–Aldrich) as a strong reducing agent.

Although sulfate reduction typically requires high temperatures to proceed efficiently, this experiment explored a low-temperature reduction process. Aluminosilicate produced through the precipitation reaction was dissolved in a small amount of water, and either 0.5 g or 1 g of $NaBH_4$ was added to the solution. The reaction was conducted at approximately 105 °C, limited by the boiling point of water. Instead of utilizing hydrothermal conditions, the experiment was conducted in an open reflux system for 24 hours under normal atmospheric pressure. The lack of an autoclave, which would have provided hydrothermal conditions, was a noted limitation in this experiment. After refluxing, the resulting precipitate was filtered, washed with distilled water, and dried overnight at 80 °C. An additional reduction test was performed by adding a few drops of formic acid to the solution along with $NaBH_4$. The inclusion of formic acid was intended to lower the pH of the solution, potentially enhancing the reduction efficiency by increasing the availability of hydrogen ions.

2.2.2 Temperature tests

Since the reduction of hackmanite using $NaBH_4$ during refluxing was unsuccessful, the necessary temperature for converting sulfate to sulfide was investigated. The aim of these temperature tests was to determine if the required temperature for efficient sulfate reduction was too high to be conducted using a reducing agent. By identifying the minimum temperature needed for this conversion, other

solvents, such as oleic acid, which can operate at higher temperatures, could potentially be considered for future experiments.

For these temperature tests, 0.5 g of hackmanite synthesized through the precipitation of an aluminosilicate solution was placed into a Lindberg furnace for reduction. The heating rate was set to 18 °C/min, and the heating time to 2 hours. The reduction temperatures ranged from 850 °C to 450 °C, with each test temperature decreasing by 50 °C. After reduction, each sample was washed with distilled water, dried, and ground in an agate mortar. These tests provided more information into the minimum temperature required to achieve a successful reduction, establishing basis for potential alternative reducing agents and reaction conditions.

2.3. Preparation of hackmanite films

Hackmanite films were prepared using tenebrescent hackmanites, which were sieved through a 25 µm sieve before film preparation to ensure uniform particle size. The film base material was silicone elastomer (Dow SYLGARD 184), composed of a silicone base and a curing agent in a 10:1 ratio. A specified amount of hackmanite was added to the silicone mixture to achieve the desired mass percentage. The resulting hackmanite-elastomer mixture was thoroughly mixed to ensure an even dispersion of hackmanite particles throughout the silicone base. The mixture was then evenly spread on a 0.1 mm thick polyethylene film (copier film), which was placed in a Memmert VO 200 vacuum oven for 10 minutes at 25 °C and 10 mbar to remove air bubbles. Finally, the films were cured in an incubator at 70 °C overnight. This curing step allowed the elastomer to set, resulting in a flexible, tenebrescent hackmanite film.

2.3.1. Optimization of the hackmanite mass percentage

At the beginning of the experiment, hackmanite mass percentages in the films were set between 5% and 0.17%, with various amounts within this range being tested. The hackmanite content was optimized based on visual inspection as well as reflectance and transmittance measurements. Hackmanite H7.5 was selected for the film fabrication process due to its small crystal size and photochromic properties, which will be analyzed in Chapter 3.1.

The initial films were prepared by first weighing 1.7 g of silicone elastomer and 0.17 g of curing agent, which were then mixed with 0.0984 g of hackmanite in a plastic beaker. Half of this initial mixture was applied onto a plastic film. Next, another 1.7 g of silicone elastomer and 0.17 g of curing agent were added to the remaining mixture. Half of this new mixture was then poured onto a plastic film. This dilution process was repeated four times, resulting in a series of five films with theoretical hackmanite mass percentages of 5.00 %, 1.70 %, 0.75 %, 0.35 %, and 0.17 %. The films were then

placed in a vacuum oven at low pressure for 10 minutes to remove air bubbles, and subsequently cured overnight at 80 °C.

During this initial series of films, the progressive dilution of the hackmanite mixture presented some challenges. It was challenging to consistently transfer exactly half of the mixture onto the film, and remnants of the previous mixture often adhered to the sides of the plastic beaker during the addition of elastomer and curing agent for dilution. As a result, the actual hackmanite content in the fourth and fifth films may deviate from the intended values. To address this issue, a new set of films was prepared individually rather than through dilution to achieve more accurate hackmanite mass per cent.

The optimization of hackmanite proportions was guided by comparing the results from the initial set of films, which will be detailed in Chapter 3.2.1. The analysis revealed that films exhibited cloudiness at high hackmanite concentrations, whereas low concentrations resulted in diminished tenebrescence properties. Therefore, the hackmanite amounts for the films were selected to be within the range of 0.35 m-% to 1.70 m-%. Hackmanite used in the previous films, H7.5, was also utilized in these films. The film preparation process involved accurately weighing 1.00 g of elastomer and 0.1 g of curing agent, mixing them in a plastic decanter with the proper amount of hackmanite for the desired mass per cent, and applying the mixture in consistent quantities evenly onto the plastic film, as done previously.

2.3.2. Aggregation control in films

Following the analysis of previous results, new films were fabricated to address the issue of hackmanite aggregation observed in the previous films, which was particularly evident in the SEM images. Two surfactants – Triton X-100, a nonionic surfactant, and Anti-Terra 250, a polymer-based surfactant – were introduced as an additive to the starting materials.

The hackmanite mass percentage in these films was set to approximately 0.70 m-%, to allow better comparison within the same film set as well as with previous films of the same hackmanite m-%. For the first film, a basic plastic transfer pipette was used to add a drop of Triton X-100 ((p-(1,1,3,3-tetramethylbutyl)phenyl)poly(oxyethylene), from Sigma-Aldrich) to the starting mixture, resulting in a relatively high Triton content of 1.10 m-%. Therefore, to improve precision, a Pasteur pipette was used in the preparation of the two following films, which allowed for more controlled and reduced volume addition. Additionally, due to the minimal amounts of Triton X-100 required, extra silicone elastomer and curing agent were added to the mixture to facilitate the attainment of this low concentration. As a result of these adjustments, the amount of Triton X-100 was reduced from 1.10 m-% to 0.12 m-% and finally to 0.06 m-%. However, because the vacuum oven was unavailable at

the time, the film with 0.12 m-% of Triton X-100 could not be placed in the oven immediately after preparation. This delay led to the formation of impurities and caused the starting materials to spread more in the plastic film before curing, resulting in less reliable measurement results and a significantly thinner film compared to the others.

The properties of the previous films led to trying if Anti-Terra 250 (BYK) could help with aggregation issues. However, the initial hackmanite had ran out, so more was synthesized using the same synthesis route as for hackmanite H7.5 (Chapter 2.2.1.). As the optical features of this hackmanite differ from the one used in the making of Triton X-100 films, another film without Anti-Terra 250 was made to see the impact of the surfactant addition, while the other had 0.10 m-% of it. The films were synthesized as described previously, and the hackmanite mass percentage was kept at 0.7 % to allow comparison.

In addition to testing surfactants, a modified dispersion technique was explored. Two hackmanite films were synthesized using hackmanite BH0.1, one by mixing the starting materials with a plastic spoon by hand, and another by using a tip sonicator (Hielscher UP100H, 125 W/cm) for 10 minutes. In order to properly dip the tip to the mixture, more elastomer was needed, as the usual amount of 1.7 g was insufficient. Thus, 10 g of elastomer, 1.00 g of curing agent and 0.19 g of hackmanite were mixed. These films were prepared following the same method described previously, with the film thickness set to 0.35 mm using a film applicator, which will be further detailed in the following chapter.

2.3.3. Optimization of film thickness

The thickness of the films was measured using a VWR International digital caliper, with measurements taken from the center of each film at a flat, even spot. These measured thicknesses include the 0.10 mm designated to the copier film that the photochromic films were prepared on, as all the measurements were conducted with the copier film included.

In the initial experiments, the film thickness varied significantly due to inconsistent amounts of the elastomer–hackmanite mixture applied to the plastic film and allowed to spread freely. During film preparation, additional silicone elastomer and curing agent were added to the mixture after the previous film to gradually dilute the hackmanite concentration. Half of this mixture was then applied to the polyester film to form a new film. As a result, the last films are slightly thicker because the increased mixture volume led to a larger amount being applied to the polyester film. Films from the second series are noticeably thicker as they were individually prepared without dilution, applying almost the entire initial mixture on the copy film. These variations in film thickness significantly affect the transmittance measurements, as thinner films appear lighter when colored, causing the

results to be incomparable. Thicker films generally exhibit lower transmittance already before coloring compared to thinner ones, regardless of the hackmanite concentration, leading to less reliable comparisons within the film series. Therefore, due to the inconsistency in film thickness, the transmittance results of the second film series are not fully comparable to those of the other films.

To address this issue, a film applicator was used to ensure more consistent thickness. Although commercial photochromic lenses typically have a thickness of 1.5 to 2.0 mm[53], the hackmanite–elastomer mixture spreads rapidly when poured onto the polyester film, requiring a thinner application. In these experiments, the film mixture was prepared as previously described and then uniformly applied onto a polyester film using an Erichsen Coatmaster 510 film applicator. The draw-down speed was set to 5 mm/s, and the application layer thickness was set to 0.35 mm, which was the average thickness of the previous films. This film applicator enabled more precise control over the film thickness, eliminating thickness as a variable factor in the final results.

2.4. Acrylic hackmanite disks

As previously discussed, some unpublished experiments in incorporating hackmanite into glass using sol-gel or melt-quenching methods had shown no success, so other ways to make transparent lenses were studied.

To explore other possible routes for photochromic hackmanite lenses, acrylic resin was tested. Hackmanite disks were prepared using Technovit 4006 resin (Heraeus Kulzer GmbH), a highly transparent, cold-embedding resin based on methyl methacrylate (MMA), with a 12-minute curing time at relatively low temperatures. This 2-component powder-liquid system is typically cured in a specialized PressurePot designated for Technovit materials, but it was not available in this experimental work. Instead, the curing process was conducted at 2.5 bar of pressure at room temperature, similar to the standard procedure, to increase the boiling point of the liquid and promote effective curing.

A relatively high amount of hackmanite was added to the resin to observe its behavior in the much thicker acrylic disks, especially in the case of color intensity. Initially, the powder and liquid resin components were mixed in a 5:3 ratio, after which hackmanite was added to achieve the desired mass percentage of 10 m-%. The mixture was then quickly transferred to a plastic mold, which was placed in a pressure vessel set to 2.5 bar for 12 minutes to cure. The volume of transferred mixture depended on the desired disk thickness – at first, a thicker disk was synthesized to observe how hackmanite interacts with the acrylic resin. Then, both thicker and thinner disks were made to evaluate the impact of thickness on reflectance, transparency, opacity, and other relevant properties.

2.5. Characterization

2.5.1. X-ray diffraction (XRD)

The structure and purity of the synthesized hackmanites were analyzed using X-ray powder diffraction (XRD) with a PANalytical Aeris diffractometer, operating at parameters of 40.0 kV and 7.5 mA, and with a PIXcel1D medipix3 detector. The measurements were conducted with Cu $K_{\alpha 1,2}$ radiation with the following settings: divergence slit of 1/4°, 13 mm mask, 0.04 rad soller collimator, 9 mm anti-scatter slit, nickel beta filter, beam limiter in the upper position, scan rate of 0.201°/s, and step size of 0.0217°.

The results were processed using the Rietveld method with the PANalytical HighScore Plus 4.9.0.27512 software, utilizing theoretical results from the PDF-4+2023 4.21.0.2 database. No other structural parameters, except for the unit cell parameters, were refined. Background and peak profiles were determined with a minimum peak width of 0.01, a maximum peak width of 1.00, and a peak base width of 2.00. Peaks were then fitted more precisely to the background, and sample purity was evaluated by comparing the experimental peaks to the theoretical data in the database.

The crystallite sizes of hackmanites were calculated by a modified Scherrer equation that takes into account instrumental signal broadening (1). The 2θ and full width at half maximum (FWHM) values of the characteristic highest-intensity hackmanite peak obtained using the HighScore Plus software.

(1) $$D = \frac{k\lambda}{\sqrt{(\beta^2 - \beta_{instr.}^2)}\cos(\theta)}$$

where

D = crystalline size (m)

k = shape factor, which is 0.9

λ = wavelength of the X-rays, which is 1.5406 x 10^{-10} m

β = full width at half maximum (FWHM, rad)

$\beta_{instr.}$ = line width (rad)

θ = peak position (°)

The instrumental line width, $\beta_{instr.}$, for the desired angle range was calculated by substituting the 2θ value obtained from the hackmanite peak into a quadratic equation (2). This equation describes the instrumental line width of the diffractometer used in this work.

(2) $\beta_{instr.} = 0.00001 \times (2\theta)^2 - 0.0008 \times 2\theta + 0.1028$

where

θ = angle range, °

$\beta_{instr.}$ = line width, °

Peak values used in the calculations, as well as the calculated crystallite sizes, are listed in **Table S2** in Supporting Information.

2.5.2. X-ray fluorescence (XRF)

X-ray fluorescence analysis was used to identify the elemental composition of the hackmanite samples. The spectrometer utilized for this purpose was PANalytical Epsilon 1, and the analysis protocol, Na 1h, involved conducting four separate measurements. These four measurements all had a specific detector mode, filter, acceleration voltage, measurement time, and measurement range, which are listed below in **Table 1**.

Table 1. *Specific settings of each measurement involved in the Na 1h program of XRF spectrometer.*

Measurement	Detector mode (resolution)	Filter	Acceleration voltage (kV)	Measurement time (s)	Measurement range (eV)
1	normal	Ag	50	120	2–34
2	normal	Cu	50	300	2–34
3	high	Al	12	180	automatic
4	high	-	10	3000	0.9–4.0

2.5.3. Reflectance

Tenebrescence properties of the samples were investigated by measuring their reflectance with Avantes AvaSpec HS-TEC spectrometer coupled to a 1000 µm VIS/NIR 0.37NA PC04 optical fiber and using Avantes AvaSoft 8.11.0.0 as the measurement software. The light source was Avantes Ocean Optics LS-1-Cal lamp when using optical fiber in an open environment, and Avantes AvaLight 14 DHc lamp when using an integrating sphere (in-house, mark and model not known). The integrating sphere was coupled to two optical fibers as previously mentioned, the other fiber being coupled to the lamp and another one to the spectrometer. The setup used in each measurement is listed in **Table S3** in Supporting Information.

Reflectance was first measured from the sample being studied, after which it was irradiated with 254 nm UVLS-24 UV lamp for five minutes for excitation. Immediately after this coloration, reflectance was measured again. The reflectance spectra measured before and after coloring were then compared to better illustrate the effect of UV exposure on the reflectance properties of the samples. For hackmanite powder measurements, magnesium oxide powder (MgO) was used as the white reference. For hackmanite films, however, a control film without hackmanite served as the white reference. This control film was created from silicone elastomer and a curing agent, following

the same preparation methods and using the same quantities of materials as the hackmanite films, but with no hackmanite added.

The color rise curves were measured with an Avantes AvaSpec HC-TEC spectrometer connected to a LOT-QuantumDesign MSH300 monochromator and a LOT-QuantumDesign LSB522 lamp and the same light source as in previous measurements, specifically the Avantes OceanOptics LS-1-Cal lamp. The color rise was measured with an Avantes AvaSpec HS-TEC spectrometer. A non-colored film was used as the white reference in the measurement, after which the film was colored for 30 minutes at a wavelength of 254 nm, with reflectance measured concurrently. The measurement time was set to 200 ms, with 10 measurements averaged. The results present the integrals of the spectra, i.e., the color intensity as a function of time.

The tenebrescence fading curves were measured using the same equipment as in the reflectance measurements, with a non-colored sample as the white reference. In this measurement, the sample was irradiated for 10 minutes with a 254 nm UV lamp, after which reflectance was measured for over an hour with integration time of 200 ms and 10 averages per measurement. The reflectance curves were integrated, and a new plot was fitted from these values to illustrate color intensity as a function of time.

2.5.4. Transmittance

Transmittance of the films was measured using the same setup, with optical fiber, as in the reflectance measurements. A control film synthesized without hackmanite was used as the white reference. In the first measurement, the film was placed 10 centimeters away from the light source, positioned next to the detector. After this, the film was exposed to 254 nm UV light for 5 minutes to induce coloring, and the measurement was repeated immediately after coloring, again 10 centimeters from the light source. To ensure consistency and accuracy, the film was always positioned in the same spot on the detector. This was important as in some samples the thickness of the film varied in different areas, which could affect the transmittance and thus the reliability of the measurement results.

2.5.5. Scanning electron microscope

Scanning electron microscope (SEM) images were acquired using an Apreo 2S electron microscope, operating at 2 kV. Powder samples were prepared by dispersing around 1 mg into 3 mL of pure ethanol, then putting a few droplets of this suspension on a SEM steel stub covered with a carbon conductive tape. Regarding the hackmanite films, a small square of such films (0.5 cm^2) was cut and placed on the top of the conductive tape.

Due to the difficult accessibility of SEM, only images of hackmanites H7.5 and H10, as well as hackmanite films 1_m0.73 and 1_m1.69, were obtained. This was done to closely examine the surface

structure of the films and the size differences of the hackmanite crystals. The SEM images were taken from a working distance of 10 mm using Everhart-Thornley and T1 detectors.

The Everhart-Thornley Detector (ETD) utilizes both secondary and backscattered electrons to generate an image that allows for the examination of the sample's topography or surface morphology. The T1 detector primarily detects backscattered electrons, which are useful for identifying elements deeper within the structure and analyzing the sample's elemental composition. In T1 images, heavier elements appear as brighter areas.

3. Results

The results are presented in chronological order in most parts, as the outcomes of each experiment served as the foundation for the following experiments, ensuring a systematic progression of the research.

3.1. Grinding set

The grinding set samples were prepared to optimize the grinding process, with the goal of achieving a small crystallite size. All hackmanite samples were washed three times with distilled water, resulting in the absence of NaBr impurity peaks in the XRD graphs. The main peak of NaBr, typically found at 29.9°, is almost imperceptible across samples. As no other impurity peaks are observed, this indicates that the samples are very pure. All samples display equivalent peaks to Br-hackmanite at 14.0°, 19.8°, 24.4°, 34.7°, 37.6°, 42.9°, and 45.4°, confirming that they all exhibit the desired sodalite structure **(Figure 2A)**.

Hackmanites H0 and H2.5 exhibit the deepest reflectance valleys **(Figure 2B)**, likely due to their large crystallite sizes **(Table 2 and Table S2, Supporting Information)**. Larger hackmanite crystals interact with light over a greater volume, which can result in less light to be reflected, but more being absorbed. This absorption results in deeper reflectance valleys. However, despite the benefits of high absorptance, within e.g. glass smaller crystallite sizes are preferred for transparency, as larger crystals can scatter light more effectively, leading to cloudy films that lack the desired transparency.

Considering both crystallite size and reflectance, hackmanite H7.5 was the most optimal sample. It has the smallest crystallite size and a reflectance valley with a reflectance value of 52.6 % at ~565 nm, indicating that approximately 47.4 % of the light is absorbed at this wavelength, which is not much less compared to the absorptance of hackmanites H0 and H2.5. Hackmanites H10 and H12.5 were in the ball mill for the longest duration, leading to relatively small crystalline sizes. However, their reflectance valleys are significantly smaller, which might be due to partial disintegration of the crystal structure in the ball mill. Consequently, these hackmanites exhibit weaker absorptance than

the others, possibly due to the impaired ability of the sulfide ion to donate electrons to the bromine vacancies as the original defect structure of the hackmanite is disrupted.

Table 2. *Average crystalline sizes calculated using the Scherrer equation. More extensive information, such as the parameters of the hackmanite main peak, is listed in* ***Table S2*** *in Supporting Information.*

Hackmanite	H2.5	H5	H7.5	H10	H12.5	H0
Average crystallite size (nm)	61.6	59.3	50.0	58.3	56.3	57.2

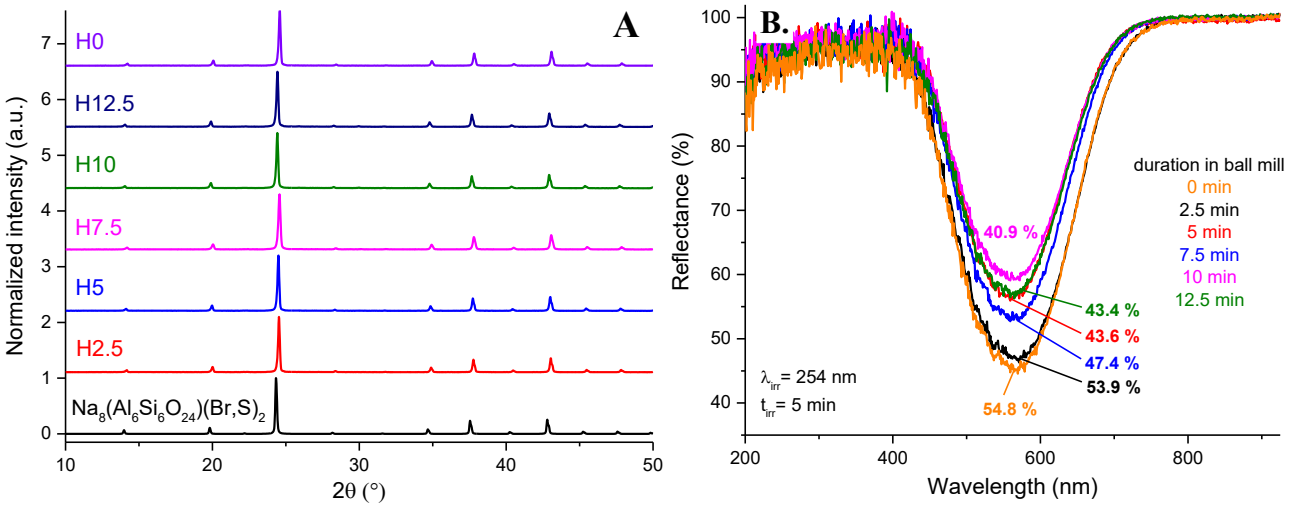

Figure 2. *XRD graphs* ***(A)*** *and reflectance spectra* ***(B)*** *of the grinding sample set. Also Br-hackmanite's ($Na_8(Al_6Si_6O_{24})(Br,S)_2$) calculated XRD graph [04-017-7137] is included from PDF4+ software. All reflectance spectra are normalized to 100 % reflectance at 900 nm, and the depths of the reflectance valleys at ~565 nm, calculated as the difference from 100 % reflectance, are reported in the figure.*

The results indicate that hackmanites H0 and H2.5 exhibit the deepest reflectance valleys, which is consistent with their larger crystal sizes. Hackmanite H5, despite its large crystal size, shows poor absorption, suggesting that size alone does not determine the absorptance efficiency. Based on these findings, hackmanite H7.5 was selected to use in film preparation, as it has the smallest crystal size in the series and relatively high absorptance.

In the SEM-ETD images of hackmanites H7.5 and H10 (**Figure 3A**–**B**), small hackmanite crystals are clearly visible, with size differences on the order of ~0.5–1 micrometer, as seen from the four-micrometer scale bar in the lower corner. When comparing the images, hackmanite H10, which shows weaker absorptance and possibly a fractured crystal structure, clearly has much larger crystal size distribution. **Figure 3C** clearly shows how the hackmanite crystals have aggregated, which is not a desirable feature for photochromic film or lens applications, where a uniform size distribution is needed, so that the color will appear uniform and not fuzzy or cloudy. In the T1 images (**Figure 3C**–**D**), distinct hackmanite crystals are visible, which, as expected, show little variation in brightness, suggesting that there is no variation in the elemental composition.

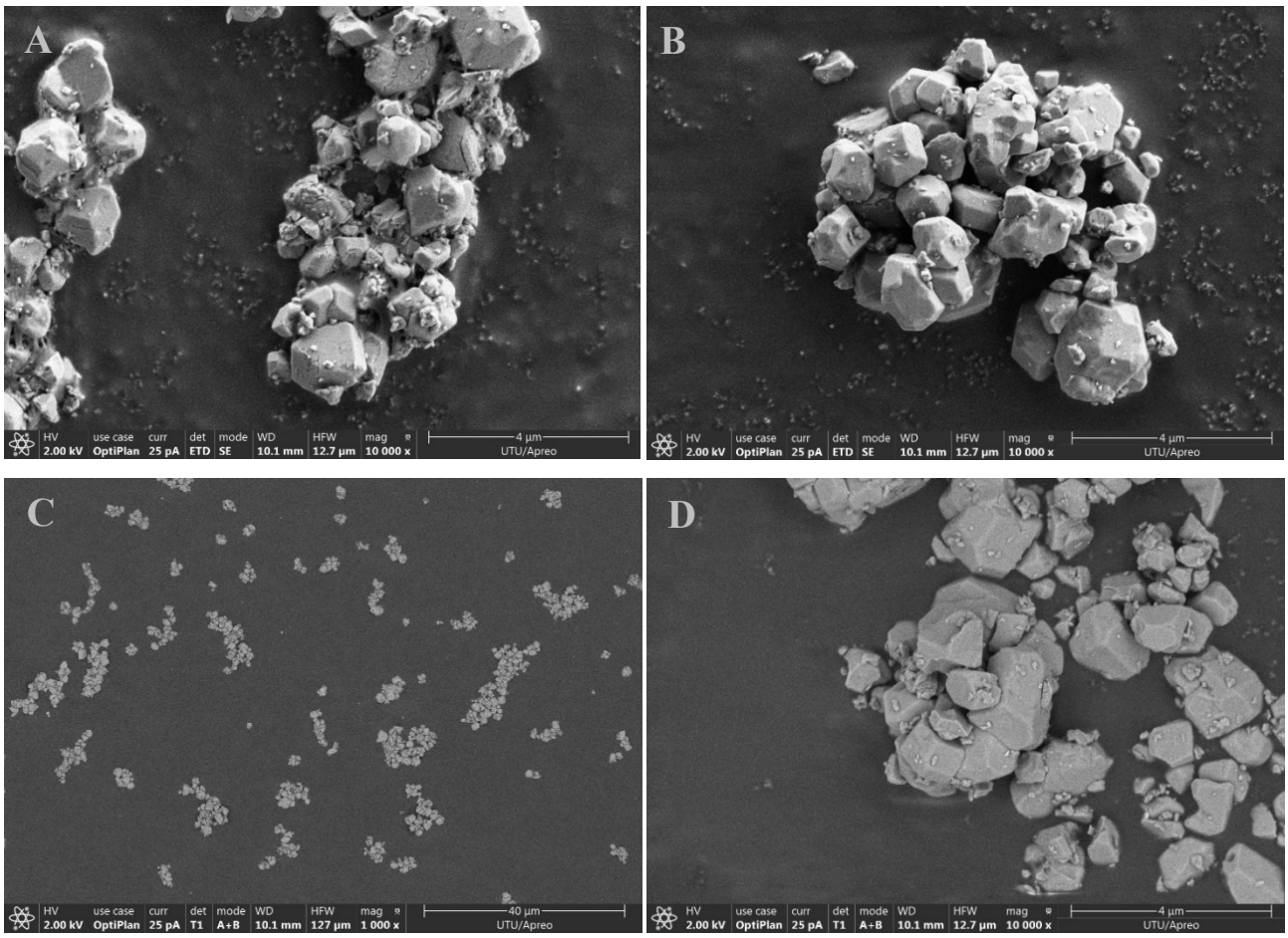

Figure 3. *SEM-ETD and SEM-T1 images of hackmanites H10 (A, C) and H7.5 (B, D).*

In addition to the tendency of hackmanite to aggregate, the large variation of the crystallite sizes should also be noticed, as this means that the crystallite size calculated from the diffraction pattern may not be completely reliable. The Scherrer equation provides the average size of the crystallites, however not accurately reflecting the larger crystals. Smaller crystals cause peak broadening in XRD diffraction peaks, meaning that the influence of large size variation isn't completely accounted in the calculations, as the FWHM would be smaller with larger crystals.[30] The differences in the calculated crystallite sizes of these hackmanites are relatively small, and due to the large error distribution, the samples' order when considering decreasing crystallite size may be completely different. However, as the crystallite sizes couldn't be calculated more accurately, H7.5 with average crystallite size of 50 nm was still chosen to be used in further experiments, as the size variation wasn't as large in the SEM images, and the absorptance was good.

3.2. Optimization of the mass percentage of hackmanite in films

Hackmanite concentration was optimized to achieve the best balance between transparency and photochromic intensity. Two sets of films were prepared: one set was prepared by diluting the starting material mixture, while the other set consisted of individually prepared films.

3.2.1. First film set

In the first set, hackmanite films were prepared by using half of the precursor mix for the initial film, while the remaining half was diluted with additional silicone elastomer and curing agent. Due to this, the calculated mass percentages may be inaccurate. The highest mass percentage was 5 %. Following the same dilution method for each film, the theoretical mass percentages were determined to be 5.00 m-%, 1.69 m-%, 0.73 m-%, 0.34 m-%, and 0.17 m-%. The film thicknesses are presented below in **Table 3**, as they significantly affect all outcomes, especially when there are substantial thickness variations within the film series. The film with hackmanite mass percentage of 1.69 is significantly thicker than the other films, but otherwise, the differences in thickness between the films are not substantial. To simplify references, the films are labeled with shorter names that indicate the film series and the hackmanite mass per cent.

Table 3. *Thicknesses of the first series of films.*

Film	1_m0.17	1_m0.34	1_m0.73	1_m1.69	1_m5.00
m-% (hackmanite)	0.17	0.34	0.73	1.69	5.00
Thickness (mm)	0.31	0.58	0.31	0.29	0.47

The depth of the reflectance valley increases with the hackmanite content (**Figure 4**). This outcome is expected, as more tenebrescent hackmanite present in the film leads to more colored material due to increased number of color centers. The most significant changes in reflectance are seen in films 1_m5.00 and 1_m1.69, likely due to the significant difference in hackmanite concentration in these films. Films with hackmanite content of 0.17 %, 0.34 %, and 0.73 % exhibit relatively small differences in concentration, resulting in smaller differences in absorption.

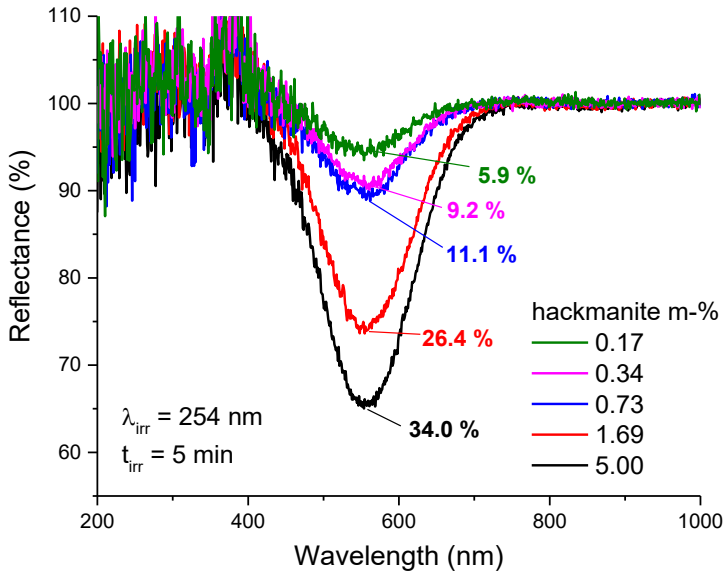

Figure 4. *Reflectance spectra of hackmanite films with varying m-%. All reflectance spectra are normalized to 100 % reflectance at 900 nm, and the depths of the reflectance valleys, calculated as deviations from 100 % reflectance, are reported in the figure.*

The transmittance spectra of the films, measured both before and after coloring, effectively illustrate the impact of UV dyeing **(Figure 6A)**. The transmittance was not measured for the films with the least and most hackmanite in the film series, as the films with the most hackmanite were quite opaque, and the films with the least hackmanite did not color much at all, which were neither desired characteristics. All samples showed the same expected behavior – the films with the most hackmanite colored the most, resulting in lower transmittance. Increasing the concentration of hackmanite intensifies both absorption and scattering, which leads to less light passing through the film. The high concentration also leads to more cloudy appearance, as the increased number of hackmanite particles reflect, scatter, and absorb light at multiple points. This is very noticeable when comparing the transparency and cloudiness of films with hackmanite content of 1.69 % and 0.17 %. When the films are held 1.5 cm above grid paper, the grid is detectable only through the film with lower hackmanite content **(Figure 5)**. Another reason for the cloudy appearance of the films is the hackmanite's behavior to aggregate.

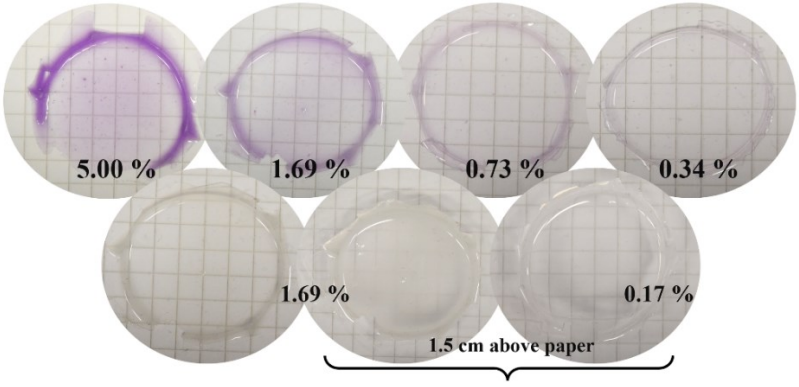

Figure 5. *Hackmanite films before (bottom) and after (top) irradiating the samples for 5 minutes with 254 nm UV light. The brightness is adjusted to enhance the distinction between the film and the white paper.*

After UV-irradiation, the lowest point on the transmittance spectra for all films was at a wavelength of approximately 510 nm, with the transmittance of about 35.0 % for film 1_m1.69, 77.4 % for 1_m0.73, and 83.4 % for film 1_m0.34, respectively. Additionally, a very small, distinct maximum at 907 nm is observed in each spectrum, which can be likely attributed to the silicone elastomer. **Figure 6A** also includes the normalized AM1.5 solar spectrum[54], which highlights how the samples particularly block wavelengths around ~415–570 nm, where the solar irradiance is the most intensive. This range also corresponds to wavelengths where the human eye is the most sensitive **(Figure 6B)**.[43,55] Therefore, photochromic hackmanite would be an excellent candidate for applications in self-adjusting eyewear.

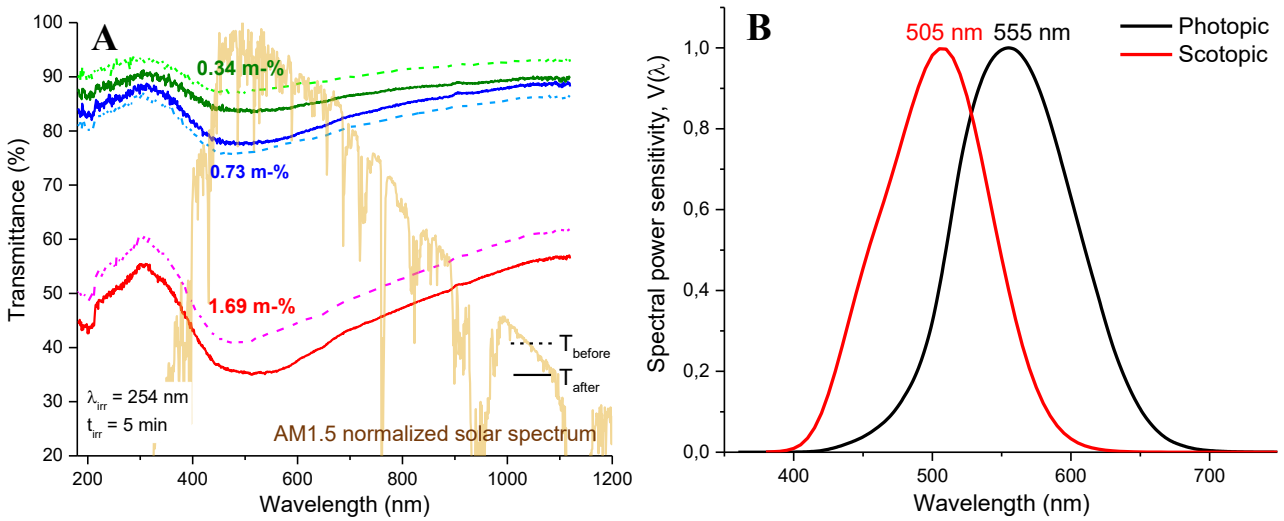

Figure 6. *Transmittance spectra of hackmanite films with varying m-% **(A)** and spectral sensitivity of the human eye adapted to daytime (photopic) and nighttime (scotopic) lighting **(B)** [56]. The m-% of hackmanite in each film is reported to the transmittance spectra.*

The surface morphology and topography of film samples are presented in the SEM images below **(Figures 7A–D)**, which visualize the issue of aggregation affecting the properties of the films. Especially in the SEM-T1 image of film 1_m1.69 **(Figure 7D)** small hackmanite crystals can be seen alongside elastomer, demonstrating the crystals' increased habit of aggregating together. Hackmanite and elastomer can be distinguished from the contrast differences: hackmanite crystals appear more lighter gray than elastomer, as heavier elements appear darker in the image. Big, aggregated clumps can be clearly seen on the right side of the image, as well as some smaller ones alongside. What should be noted in these figures, is that the scale bar is up to forty micrometers, while in the SEM images of hackmanite crystals **(Figure 3)**, the scale bar was only four micrometers, and the crystals still appeared quite large. Considering the fact that the imaging scale is increased from four to forty micrometers, it can be noted how large the aggregated hackmanite-elastomer clumps actually are – for example, in **Figure 7C**, the aggregate is more than 40 micrometers in length. Such large aggregates naturally lead to more opaque films by increasing the scattering of light. It is to be noted that **Figure 7B** shows also a big hexagonal crystal that is so far unidentified in composition.

The key finding from these SEM images is the aggregation of the crystals, which led to the production of a third film series, where Triton X-100 was added to prevent this aggregation. Further results of that film series are analyzed in **Chapter 3.4.**

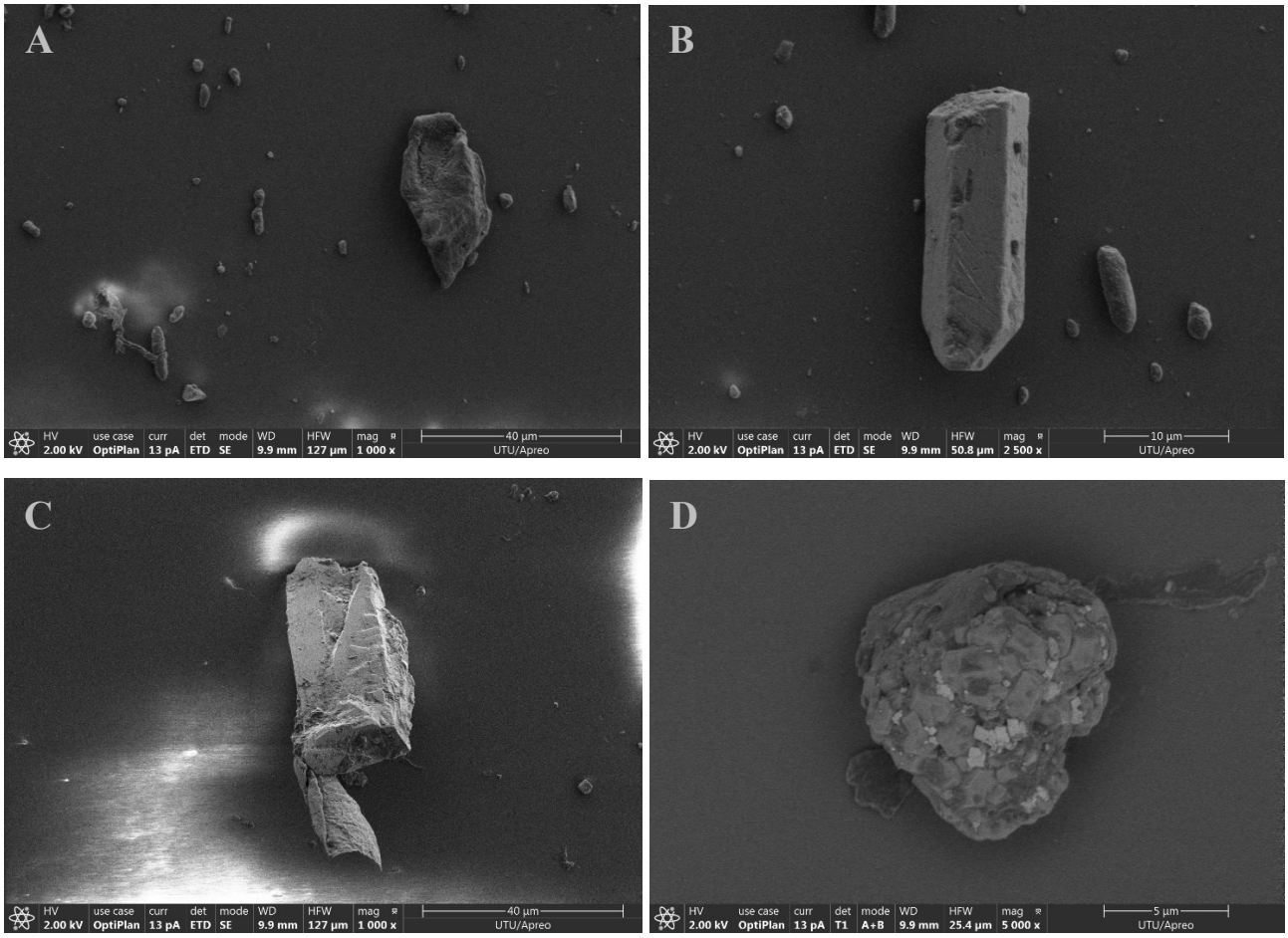

Figure 7. *SEM-ETD images of film 1_m0.73* ***(A and B)*** *and film 1_m1.69* ***(C)****, and SEM-T1 image of film 1_m1.69* ***(D)****.*

3.2.2. Second film set

The films of the second set were made individually rather than through dilution. The thicknesses of these films, compiled to **Table 4** below, were much higher compared to the first set of films, affecting especially the transmittance more. Comparing the depths of the reflectance valleys reveals that, as seen before, the tenebrescence properties are better in films with higher hackmanite concentrations (**Figure 8A**). When comparing the absorptance of these films with the previous film set, it is evident that the differences in absorption are significantly smaller when the hackmanite concentration does not vary as widely between films. In the first film series, the difference in hackmanite content between films with the most hackmanite is approximately 3.30 percentage points, whereas for these films, the difference is only 0.30 percentage points. This explains the reduced variability in the results.

Table 4. *Thicknesses of the second series of films.*

Film	2_m1.60	2_m1.29	2_m1.01	2_m0.72	2_m0.40
m-% (hackmanite)	1.60	1.29	1.01	0.72	0.40
Thickness (mm)	0.49	0.55	0.53	0.53	0.57

The transmittance of the films having the highest and lowest hackmanite m-% were left unmeasured, like in the previous film set. The lowest point on the transmittance valley after irradiation

is located at a wavelength of approximately 480 nm **(Figure 8B)**. The transmittance after irradiation is about 45.5 % for film 2_m1.29, 50.1 % for film 2_m1.01, and 60.7 % for film 2_0.72. These measurements also reveal a small, distinct peak at 907 nm, likely caused by the silicone elastomer. While the films effectively block the wavelengths below 500 nm, the transmittance remains relatively low at wavelengths above 500 nm, where both spectral solar irradiance and human eye sensitivity are particularly high **(Figure 6)**. This behavior suggests that the films offer broad-spectrum UV blocking, extending into visible light, which may be beneficial for applications requiring enhanced UV and high-intensity light protection. The decrease in transmittance with increased film thickness is particularly evident when comparing the film's transparency when placed directly on paper versus when it's positioned 1.5 cm above it **(Figure 8C)**.

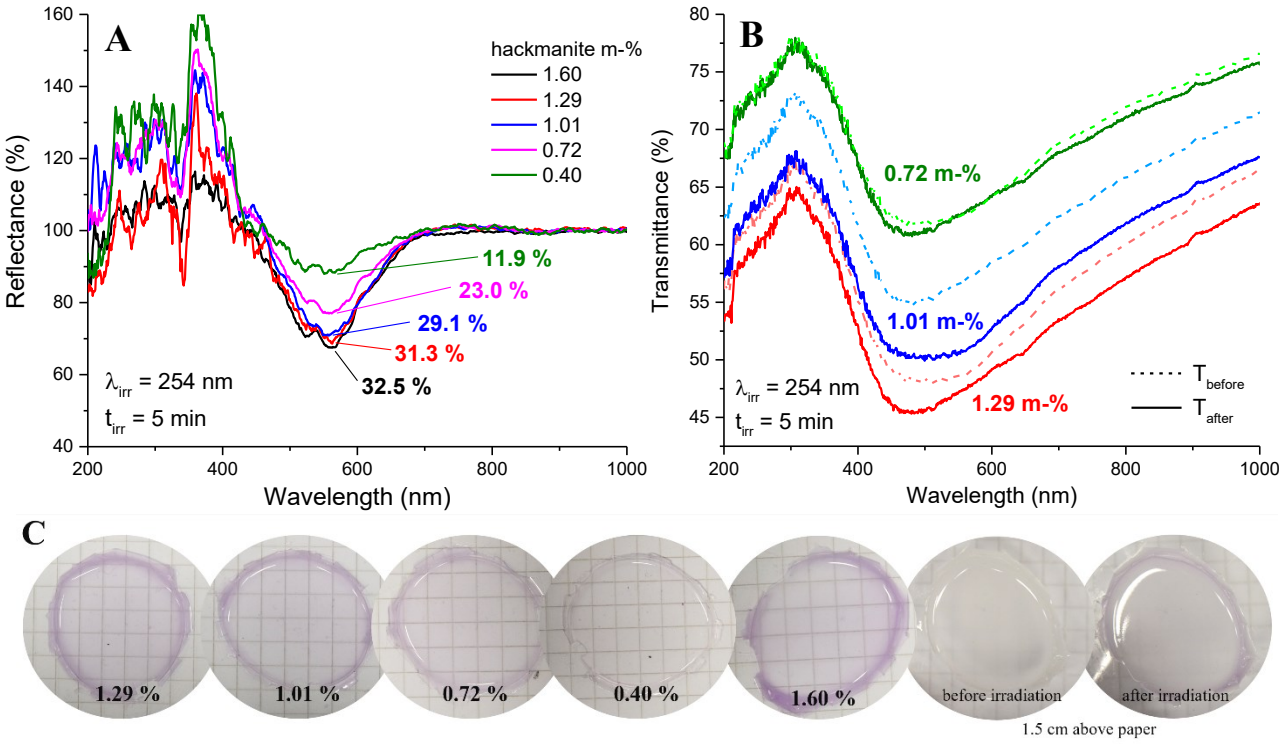

Figure 8. *Reflectance* ***(A)*** *and transmittance* ***(B)*** *spectra, and images* ***(C)*** *of hackmanite films with varying m-%. All reflectance spectra are normalized to 100 % reflectance at 950 nm, and the depths of the reflectance valleys at ~558 nm, calculated as the difference from 100 % reflectance, are reported in the figure. In transmittance spectra the m-% of hackmanite in each film is reported in the figure. The brightness of the images is adjusted to enhance the distinction between the film and the white paper, and the hackmanite m-% in each film is reported in the figure. The last three images are taken of the same film.*

The properties of the films of both series seem to behave as expected. For example, film 2_m0.40 has a little deeper reflectance valley than film 1_m0.34, as it has just a little higher hackmanite concentration and about as thick film. Between films 1_m0.73 and 2_m0.72 there is a large difference between the reflectance valley depths, but it can be explained with the film thickness – film 2_m0.72 has 11.9 percentage points deeper valley, but it is also 0.22 mm thicker. The same behavior is present with all films, thicker films exhibit more intense photochromism than corresponding thinner films with quite the same hackmanite content.

Between the film sets, there is also variation between the points of the smallest transmittance. In the first film set, the smallest transmittance is at ~210 nm, while for the other film set it is at ~480 nm. This could be due to the difference in their preparation, as the films of the second set were prepared individually rather than by dilution, like the first films. This better mixing would allow more uniform dispersion, in addition to the much shorter preparation time when compared to that of the first films, as when preparing films via dilution, the mixture was left in the decanter each time additional elastomer and curing agent were weighed for addition. Better particle dispersion together with the thicker film could result in less interference and increased interaction with the light, leading to smaller transmittance minimum.

By comparing the characteristics of films from both sets, it can be observed that the thicker films have both better absorptance and smaller transmittance relative to the hackmanite concentration. However, the films still appear very opaque, which is often attributed to light scattering, which is probably the case here also. To obtain transparency, this scattering must be minimized. In order to enhance the transparency, smaller particle size should be achieved, together with minimal particle aggregation and better particle distribution in the film or other matrices.

3.3. Coloration

To better evaluate hackmanite's suitability for photochromic applications, the tenebrescence fading rate, and the rate of coloration were measured. The color rise curves were measured for both hackmanite (H7.5) and hackmanite film (1_m5.00) to see the influence of the silicone elastomer and other properties on coloration rate **(Figure 9)**. The hackmanite and films exhibited the most intensive coloration when irradiated with a 254 nm UV lamp, which was therefore used for these measurements, consistent with all the previous experiments. The color rise curves present the color intensity as a function of time, and the difference in coloration rate between the two samples is minimal.

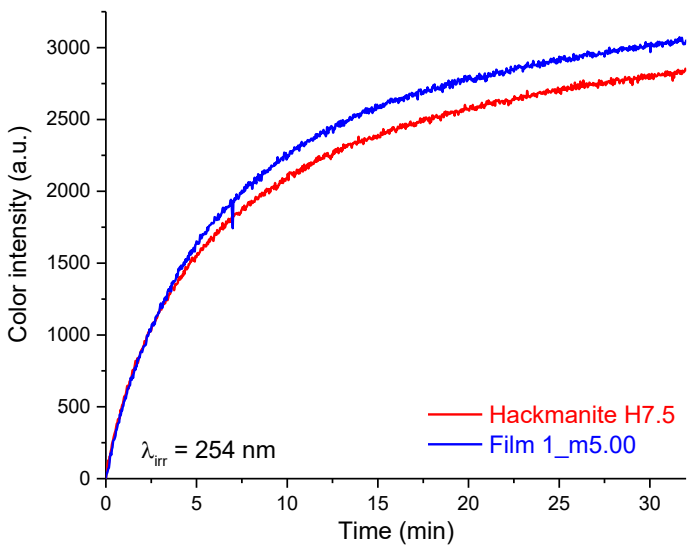

Figure 9. *Color rise curve of hackmanite and photochromic film.*

The color intensity increased over time, with the film reaching a stable coloration state in approximately 20 minutes, and the hackmanite in about 12 minutes, as indicated by the lifetimes obtained by fitting to a two-term exponential function (ExpDec2 function in OriginLab Origin) **(Table 5)**. This indicates that the hackmanite powder reaches its maximum color intensity faster

than the film, likely due to more direct UV interaction and the absence of silicone elastomer, which could slow down this process. Although the hackmanite powder reached maximum color intensity more quickly, the film maintained a more consistent, intensive color over time.

The longer coloration time of the film is not quite optimal considering its suitability for applications in photochromic eyewear, as commercial eyewear typically reaches the full color upon exposure to UV radiation within approximately 30 seconds to 2 minutes, despite having an average thickness of 1.5–2 mm – considerably thicker than the films prepared in these experiments.[44,53], However, as this study is just preliminary experimentation focusing on the potential use of hackmanite in eyewear, the results are not expected to compete with those of commercial eyewear. Additionally, the silicone elastomer in these films has limited absorptance and transmittance properties, further reduced by the elastomer's tendency to collect dust and impurities due to its sticky surface, as well as uneven hackmanite distribution, as discussed previously.

Table 5. *ExpDec2 parameters of color rise curves. Smaller t1 values indicate a faster initial rise in color intensity, while larger t2 values indicate a longer coloring phase. Higher A values indicate a more noticeable color intensity rise during the process.*

	t_1 (min)	t_2 (min)	A_1 (a.u.)	A_2 (a.u.)	y_0
1_m5.00	4.1 ± 0.1	22.3 ± 1.6	-1762.2 ± 52.1	-1629.8 ± 20.8	3451.6 ± 38.9
H7.5	2.6 ± 0.0	13.3 ± 0.2	-1061.2 ± 14.8	-1873.7 ± 11.9	2995.2 ± 4.9

The tenebrescence fading curves **(Figure 10)** were measured for only five films due to the longer measurement process, which limited the number of samples that could be tested. Based on the previous results, the second set of films displayed slightly better properties, so four films from this set and one film from the first set were chosen for measurement. Films 2_m1.60 and 2_m1.29 showed the fastest fading at the beginning of the measurement, which is likely due to their higher hackmanite m-%, resulting in more intense shade of violet color.

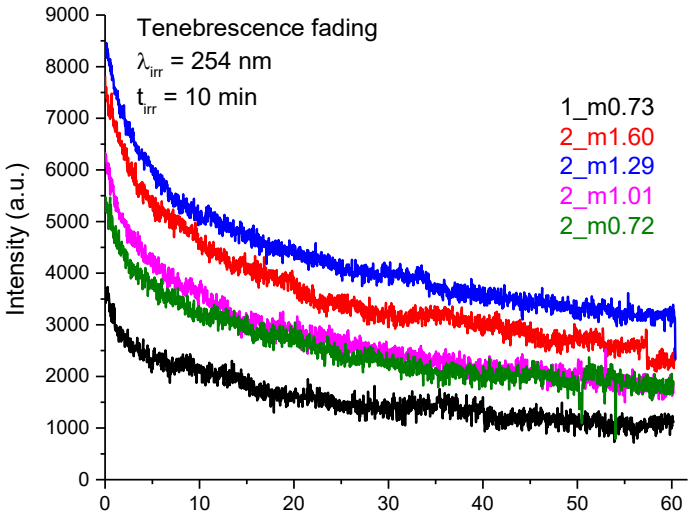

Figure 10. *Tenebrescence fading curves of films listed in the figure.*

From the lifetime parameters of the fading curves, listed in **Table 6** below, the fading rate can be seen to be directly dependent on the hackmanite concentration. Films with higher hackmanite concentration fade more slowly when compared to films with lower concentration, such as films 1_m0.73 and 2_m0.72, which fade more quickly. However, the films with higher hackmanite

concentration have a more intense coloration, meaning the color also fades more noticeably over time. This is expected, as films with lower concentration fade more quickly and less intensively. These results are as expected, as films with lower hackmanite content also have fewer bromide vacancies, resulting in less color centers and, consequently, less substantial color change. The time required for fading to occur is significantly longer than the time for coloration, due to the unfavorable quantum mechanical transition that is necessary for the electrons to recombine with the S_2^- ions.[4] So, when the number and density of the color centers is higher, the fading process proceeds much slower due to the increased number of electrons requiring recombination with the S_2^- ions.

In the initial phase, the fading rate for all films ranges from 1.15 to 5.43 minutes, which is promising for potential use in photochromic eyewear, as the fading is expected to occur rather quickly when going indoors. However, the second, slower fading phase (t2) is notably long even for films with lower hackmanite m-%. The initial color intensity drops quite fast, but complete fading of the color takes significantly longer than the 5–10 minutes typical for commercial photochromic eyewear[50,53]. This tenebrescence fading speed could however be improved if the hackmanite was embedded in a different base material, such as glass. The silicone elastomer isn't completely clear even without the hackmanite, so measuring the fading curve of a more transparent sample with hackmanite could provide more reliable results. Additionally, measuring the fading curve of hackmanite powder would have allowed comparison of how the elastomer affects the fading process, but this was not included in this study as it was realized only later.

Table 6. *ExpDec2 parameters for tenebrescence fading curves. Smaller t1 values indicate a faster initial drop in color intensity, while larger t2 values indicate a longer fading phase. Higher A values indicate a more noticeable fading effect during the process.*

Film	t_1 (min)	t_2 (min)	A_1 (a.u.)	A_2 (a.u.)	y_0 (min)
1_m0.73	1.2 ± 0.1	22.3 ± 0.7	999.2 ± 42.9	1777.9 ± 15.4	15.8 ± 0.3
2_m1.60	5.4 ± 0.2	59.0 ± 7.9	2667.5 ±76.9	3500.6 ± 158.2	19.4 ± 3.9
2_m1.29	3.2 ± 0.1	33.0 ± 1.1	2513.7 ± 35.7	3285.0 ± 19.3	43.5 ± 0.6
2_m1.01	3.2 ± 0.1	28.6 ± 1.1	1827.9 ± 42.5	2769.1 ± 23.9	24.9 ± 0.5
2_m0.72	1.6 ± 0.1	20.6 ± 0.5	1209.5 ± 40.8	2575.6 ± 20.8	28.0 ± 0.3

3.4. Aggregation control in films

Because of the aggregation observed in the results presented above, possible means of reducing clumping were investigated. The third set of films, prepared to experiment if Triton X-100 would solve this problem with hackmanite aggregation in films, consisted of three films which all had hackmanite concentration of 0.70 %, while the mass percentage of Triton X-100 varied (**Table 7**). In the reflectance measurements of these films, a film containing Triton X-100 and no hackmanite was used as the white reference instead of a film without hackmanite, like was done with the previous films. This allowed the reflectance contribution from both Triton X-100 and silicone elastomer to be

excluded when subtracting the reflectance values measured before dyeing from the ones measured after dyeing. The reflectance spectra **(Figure 11A)** clearly demonstrate that the reflectance valley of film Triton0.12 is significantly smaller compared to the other two films, most probably due to the poor manufacturing process. The reflectance valleys of films Triton1.10 and Triton0.06 are quite as deep, indicating that inclusion of Triton X-100 does not significantly reduce the photochromic behavior. The difference between the valleys is only about one percentage point, which could be attributed to factors such as varying film thickness due to film preparation without the film applicator, minor impurities, or uneven distribution of hackmanite within the film. Thus, it could be stated that in the case of UV absorption, Triton X-100 is a safe additional reagent to use in aggregation control in making of hackmanite films.

Table 7. *Mass percentages of hackmanite and Triton X-100, and thicknesses of each film.*

Film	Triton1.10	Triton0.12	Triton0.06
m-% (hackmanite)	0.70	0.70	0.70
m-% (Triton X-100)	1.10	0.12	0.06
Film thickness (mm)	0.48	0.16	0.51

Film Triton0.12 exhibits significantly higher transmittance compared to the other films **(Figure 11B)**, but this film was also considerably thinner and did not undergo intense coloration under the UV lamp. Additionally, there is a notable difference in transmittance between films with Triton m-% of 1.10 % and 0.06 %, despite both having the same hackmanite concentration. Films Triton0.06 and Triton1.10 are quite similar in thickness, but film Triton1.10 transmits light much less effectively. This reduced transmittance may suggest that higher concentration of Triton X-100 does not help with aggregation but instead enhances it. It could also be due to impurities or air bubbles in the area of the film where transmittance was measured. The opacity and lack of transparency of the films, especially when held few centimeters above the grid paper, are illustrated in **Figure 11C**.

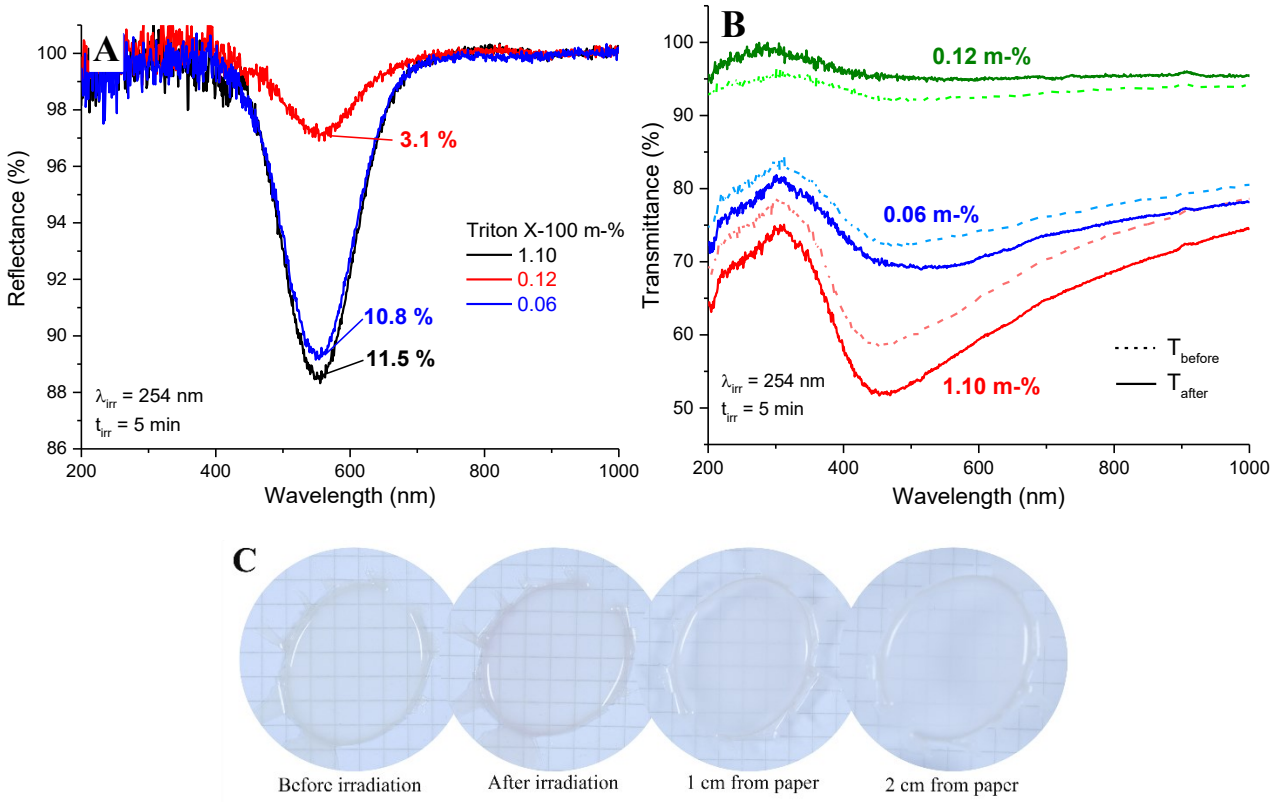

Figure 11. *Reflectance (**A**) and transmittance (**B**) spectra, and images **(C)** of hackmanite films with varying Triton X-100 m-%. All reflectance spectra are normalized to 100 % reflectance at 950 nm, and the depths of the valleys at 554 nm, calculated as the difference from 100 % reflectance, are reported in the figure. In transmittance spectra the m-% of Triton X-100 in each film is reported in the figure. The images are all taken of film Triton1.10, and due to much brighter lighting, the film may appear lighter in color compared to the previous images of other films.*

Films with 1.10 m-% and 0.06 m-% of Triton have better transmittance before dyeing, which is the expected outcome for transparent or -lucent materials intended to color under UV exposure. After dyeing, the transmittance minimum of film Triton1.10 is 51.9 % at 467 nm, and 69.0 % of film Triton0.06 at 515 nm. Film Triton0.12 showed improved transmittance after dyeing with the transmittance minimum being approximately 95.2%. This result is not ideal, as the transmittance of the film is expected to decrease when colored. However, this unexpected increase in transmittance might be attributed to several factors related to the measurement setup, as it was not done in a covered area. Although the transmittance was measured in a dark room, with only the light from the computer screen and the light source directed at the film, there may have been other sources of stray light affecting the results. For instance, reflections from the computer screen, the measuring equipment, or even from a white laboratory coat could have influenced the measurements. Additionally, variations in the alignment of the film relative to the light source and the detector, as well as slight inconsistencies in the positioning of the film, could have caused errors. The ambient light could have interacted with the surface of the film, especially given its varying thickness and the potential presence of air bubbles or impurities as the films collect also dust very easily.

Films Triton0.06, Triton1.10 and 2_m0.72 all have quite the same thicknesses, but the UV absorption of film 2_m0.71 is much more intensive, as the reflectance valley is around 10 percentage

points deeper. Due to the better absorption, it could be expected that film 2_m0.71 would also have a smaller transmittance minimum, but it is however only slightly better than that of film Triton1.10. This could indicate that including Triton X-100 in the film does not help with the aggregation, especially as the better transmittance of Triton0.06 is most likely due to smaller Triton content. The very good transmittance of film 1_m0.73 can most likely be attributed to no Triton in the film, much less thick film, and smaller reflectance valley, which leads to less intense color. SEM-ETD images taken of the film Triton1.10 **(Figure 12A**–**B)** confirm this theory by showing that even though the surfactant nature of Triton X-100, it could not prevent the hackmanite aggregating together with the elastomer. Especially on a larger scale, the big, aggregated hackmanite–elastomer clumps can be seen **(Figure 12B)**.

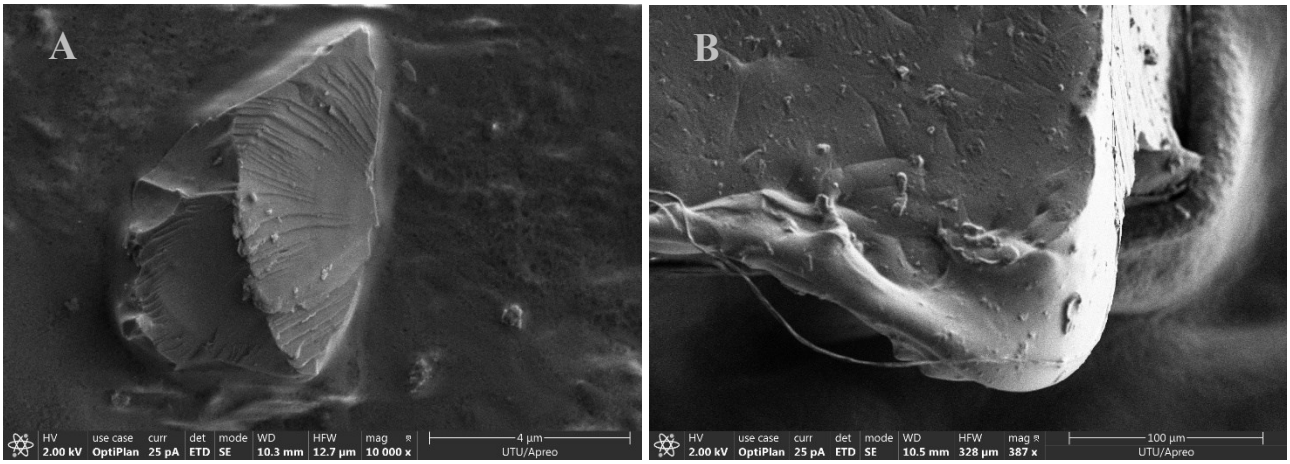

Figure 12. *SEM-ETD images of film Triton1.10 with a four (A) and one hundred (B) micrometer scale provided in the lower right corner.*

In addition to Triton X-100, also Anti-Terra 250 was used to help with aggregation. As the reflectance valley of the synthesized hackmanite is much smaller compared to the hackmanite used in the Triton films, also the absorptance of these films is naturally much smaller **(Figure 13)**. The key point is however the large difference, about five percentage points, in the measured reflectance between the films. The film with the added Anti-Terra has a much smaller valley, which could also be seen by the eye as lack of color. This could not be explained with large thickness differences, as film applicator was used, leading a thickness of 0.27 mm for the reference film, and 0.25 mm for the film with Anti-Terra. Due to this, no further measurements or experiments were conducted with the surfactant.

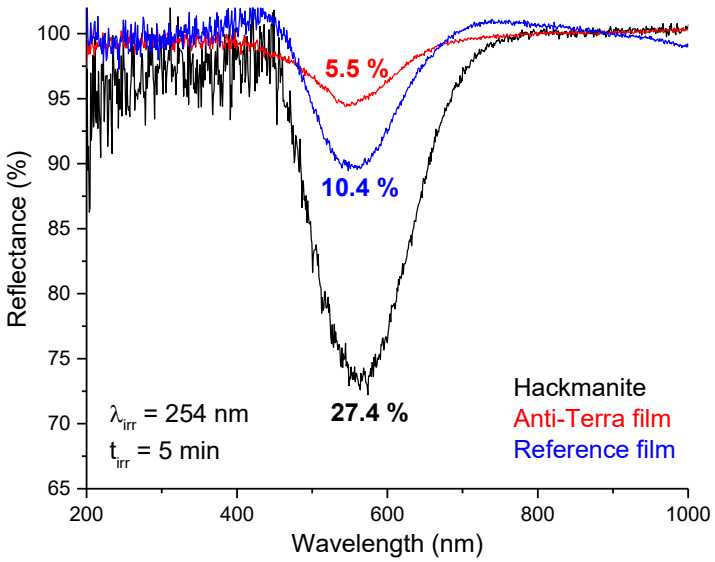

Figure 13. *Reflectance spectra of the film with Anti-Terra 250, the reference film, and the hackmanite used in them. All spectra are normalized to 100 % at 900 nm, and the depths of the valleys at 560 nm, calculated as the difference from 100 % reflectance, are provided in the figure.*

Given the type of surfactants, Anti-Terra 250 could have been expected to be a better option concerning this aggregation control, as Triton X-100 offers better help mostly when wanting to reduce surface tension to solubilize hydrophobic substances in water. Also, nonionic surfactants are more sensitive to high temperatures, as when heating, the surfactant solutions become cloudy. This so-called cloud point temperature of Triton X-100 is around 66 °C in water, and even though the films were made of elastomer mixture and not in an aqueous solution, they were still left at 70 °C overnight.[57] This has probably played a small part in the increased cloudiness of the film, as the Triton X-100 might have affected the curing process. In the case of Anti-Terra 250, the reduced UV absorption might have been due to reduced exposure of hackmanite particles to UV light due to morphological reasons, such as decreased particle dispersion, for example. Another possible reasoning for the decreased absorptance, is Anti-Terra coating the hackmanite particles and thus limits the excitation of the valence electron of S_2^{2-} to the bromide vacancy. This would lead to a smaller number of color centers and thus less effective photochromic response to UV light. This could be further investigated with SEM, but in this research the limited availability of SEM limited the number of samples to examine, so these films were not studied any more.

In addition to testing dispersing agents, the dispersion technique was tried to be improved by using a tip sonicator instead of just mixing the mixture with a plastic spoon. However, both the reference film and the sonicated film have relatively small reflectance valleys **(Figure 14)**, considering that the films in the Anti-Terra 250 and Triton X-100 experiments all had 0.7 m-% of hackmanite, meanwhile these films had 1.7 m-%, and still the valleys were as deep. The reason for this could be smaller UV absorption of the used hackmanite, but the hackmanite used in this experiment was BH0.1, which had

even deeper reflectance valley **(Figure 16**, 36.8 %) than the hackmanite used in the making of the Anti-Terra film and its reference **(Figure 13**, reference film 10.4 %).

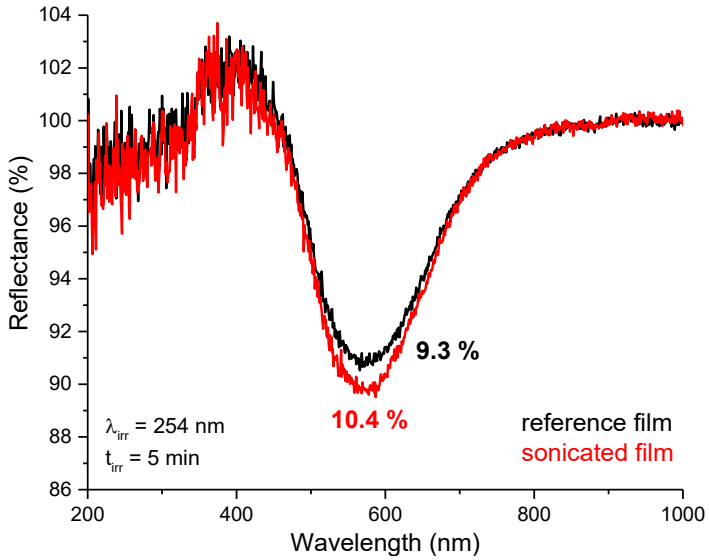

Figure 14. *Reflectance spectra of the sonicated film and the reference film. Both spectra are normalized to 100 % at 1000 nm. The depths of the valleys, calculated as the difference from 100 % reflectance, are provided in the figure.*

Neither the thickness differences between the films can explain the weak absorption despite the higher hackmanite m-%. A film applicator was used, leading to a thickness of 0.35 mm for the sonicated film, and 0.36 mm for the reference film, meaning that they are about 0.10 mm thicker than the Anti-Terra reference film, but over 0.10 mm thinner than the Triton1.10 and Triton0.06 films. Despite the large thickness variation between the films, the reflectance valley was around 10 % for each. Another explanation for the reduced UV absorption of these films was that the available tip sonicator needed a lot of mixture to properly work, as it was not made for smaller quantities. This meant that a lot of hackmanite was needed to achieve a high m-%, which was needed to see the influence of sonication on the film's properties. The relatively low UV absorption and thus quite nonexistent color change could be due to partial destruction of the hackmanite structure during the sonication, or inefficient mixing of the hackmanite–elastomer mixture. As over 10 grams of elastomer was used in the mixture and only a small part was used in the making of the film, the hackmanite may have been aggregated in the part of the mixture that was not used.

Despite the potential of especially Anti-Terra 250, the experiments with aggregation control were not continued anymore. Using a tip sonicator, as well as the inclusion of Triton X-100 and Anti-Terra 250 reduced the wanted features such as transmittance or UV absorption, without showing any significant help in the problem with aggregation. Thus, more focus was put on other parameters that could be improved and explored, such as the synthesis parameters.

3.5. Addition of boron

The addition of boron was investigated to explore whether it could produce hackmanite glass by modifying the solid-state synthesis route established by R. Radler.[51] All boron-containing samples have distinctive hackmanite peaks at 14.0°, 19.8°, 24.3°, 34.7°, 37.5°, and 42.8° **(Figure 15).** The H-76-11, BH0.05, BH0.1, BH0.14, and BH0.17 samples are all very pure, with no impurity peaks observed. However, the H-11-S-3 sample shows several additional peaks that correspond to the XRD pattern of nepheline ($Na_3KAl_4(SiO_4)_4$). The four main peaks of nepheline, located at 21.3°, 23.2 °, 27.3°, and 29.8°, are clearly detected in the XRD pattern of H-11-S-3, along with several other peaks of lower intensity. This indicates the presence of two phases in the H-11-S-3 sample: hackmanite and nepheline.

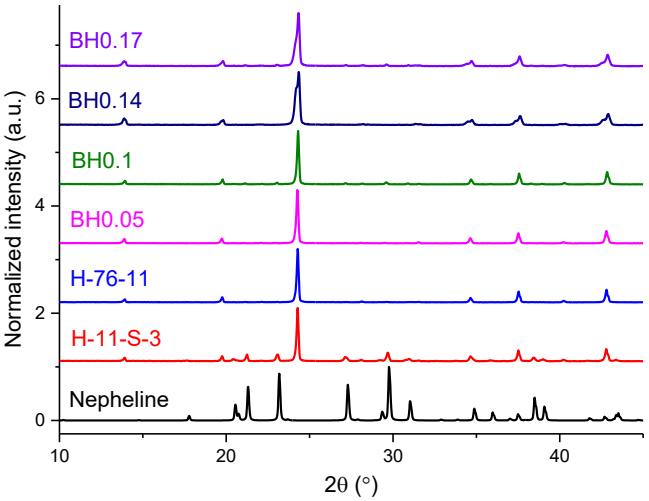

Figure 15. *XRD patterns of hackmanites with added boron. Nepheline's ($Na_3KAl_4(SiO_4)_4$) calculated XRD graph [04-016-1737] is also included from PDF4+ software.*

This inclusion of nepheline in H-11-S-3 can be attributed to the high synthesis temperature, as the used starting materials and quantities were identical to those used in sample BH0.1, yet the differences in the XRD patterns are significant. The high synthesis temperature of 1100 °C results in loss of bromide, as it can vaporize at relatively low temperatures due to its low boiling point. This loss of bromide from the structure results in the formation of nepheline alongside hackmanite. As the H-11-S-3 sample was synthesized with a much shorter reduction time and without a separate annealing step, complete loss of bromide did not occur, as the calculated XRF results **(Table S4, Supporting Information)** show that there was still nearly 27 % of Br left. The amount of Si and Al, elements much present in nepheline, is much higher, meanwhile the amount of S and Br, only in the hackmanite structure, is reduced. Together with the XRD pattern, this underlines the formation of nepheline.

The different reaction conditions may have also affected the overall progress and completion of the reaction. In addition, as the dwelling time was relatively short, only 30 minutes, some bromide might have left in the product as NaBr impurity, not being able to take part in the forming hackmanite structure. Even though Zeolite 4A ($NaAlSiO_4$), which was used as a starting material, does not have potassium, some potassium is expected to result from impurities. All these may have resulted in the formation of potassium-containing nepheline in the H-11-S-3 sample. Sample H-76-11, also synthesized in such high temperature, did not have additional zeolite as a starting material as it was substituted with already synthesized hackmanite. Due to this, there is no nepheline formed.

Sample H-11-S-3 exhibits the deepest reflectance valley, with a difference of nearly 10 percentage points compared to H-76-11, which has the shallowest valley **(Figure 16)**. Notably, out of the four samples – BH0.05, BH0.1, H-11-S-3, and H-76-11 – synthesized in the beginning of the study of boron impact, H-11-S-3 contains the highest amount of boron, like sample BH0.1. In contrast, sample H-76-11 has the lowest boron content and the smallest reflectance valley. These results suggest that the inclusion of boron appears to increase the depth of the reflectance valley, resulting in enhanced absorptance. However, the samples BH0.14 and BH0.17, which were synthesized to explore this enhancement, showed a color change only hardly visible by naked eye, and the shrinkage of the reflectance valley depth is very significant when compared to other samples. This suggests that the optimal boron trioxide content is specifically around 0.1 g, and adding more will result in loss of photochromic effect. This could be due to unfavorable changes in the structure of the material. Excessive amount of B_2O_3 could alter the hackmanite structure, causing disruption in the crystal lattice and preventing the formation of the defects that are essential for the photochromic effect in hackmanite.

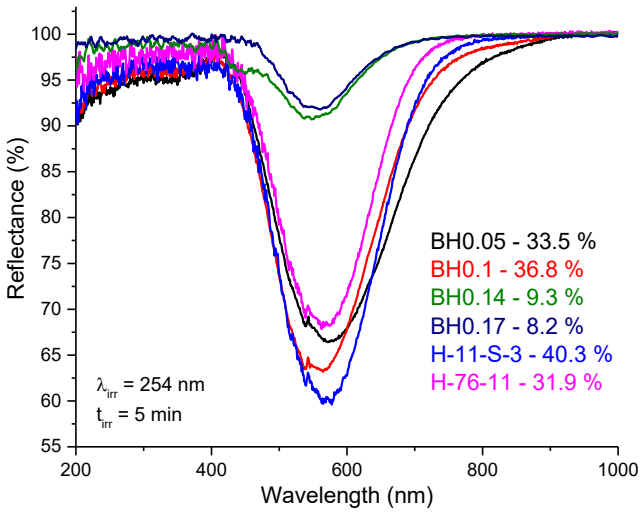

Figure 16. *Reflectance valleys of hackmanites with added boron. All reflectance spectra are normalized to 100 % reflectance at 950 nm, and the depths of the valleys are included in the figure.*

Another possible explanation for the loss of photochromism in these samples is boron reacting together with the starting materials, such as sodium, and forming separate compounds, such as sodium borate. This would reduce the amount of sodium available for hackmanite formation, naturally leading to loss of photochromism. Both samples also have higher amounts of sulfur, BH0.14 having 1.70 % and BH0.17 having 1.38 % **(Table S4, Supporting information)**. This is a significant increase, as the amount of sulfur is much below 1 % in almost all the hackmanite samples synthesized in this study. The amounts of other elements didn't significantly differ from those of samples BH0.05 and BH0.1, which both had better absorptance. The higher amount of sulfur, together with the weak photochromism, could indicate that the synthesis reaction wasn't complete, and all of the sulfate was not reduced nor taking part of the hackmanite structure. The reduction process did not necessarily proceed as wanted, if the gas supply was discontinuous. B_2O_3 is also a very strong fluxing agent, so the high amount of it combined together with the high synthesis temperature may lead to excessive melting of the mixture. This could result in the loss of stoichiometry, together with the earlier described possible formation of e.g. borates.

When comparing the results with those from the grinding set samples, even the deepest reflectance valley in boron-containing samples is notably smaller, only 40.3 %. This could indicate that the addition of boron diminishes the depth of the reflectance valley. Nevertheless, within the set of boron-containing samples, boron seems to deepen the valley, suggesting that boron might not be the sole factor responsible for the diminished valley depth. Instead, differences in the starting material quantities between the grinding set samples and the boron-containing samples could be contributing factors. Specifically, in the boron-containing samples, the amount of added NaBr was more than 2.4 times smaller, and the amount of Na_2SO_4 was nearly 1.5 times smaller, while the amount of zeolite remained almost the same in both sets.

The color change of samples BH0.14 and BH0.17 is very weak, and the color contrast between them and the other boron samples is very distinctive **(Figure 17)**. The purple color of all the samples H-11-S-3, H-76-11, BH0.05 and BH0.1 can be seen by naked eye very well, as well as the slight variation in their contrast. Even though the pastel purple color is quite intensive, it is still much less intense than when comparing with, for example, the colors of reduction temperature test hackmanites **(Figure 20)**.

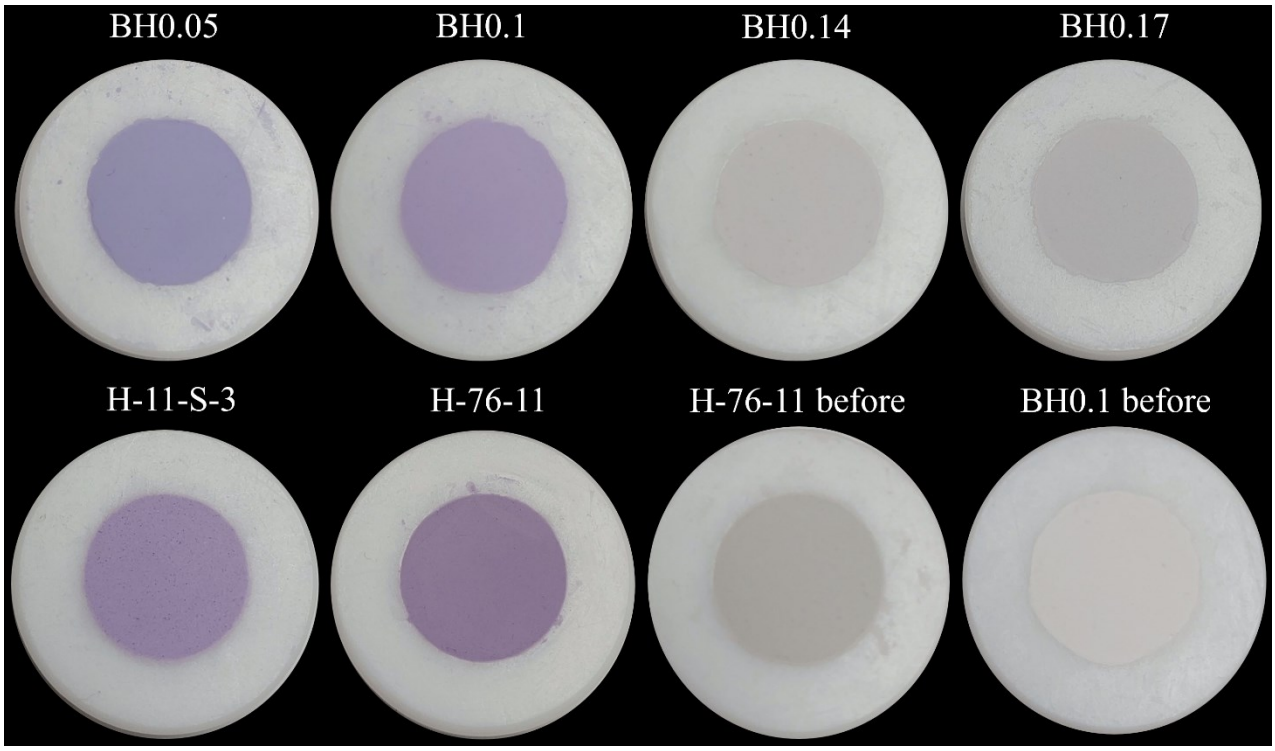

Figure 17. *Pictures of the boron hackmanites. The pictures were taken after irradiating the samples for 5 minutes with 254 nm UV radiation, and the contrast of the pictures was adjusted to enhance the distinction between the colored material and the white holder. Unlike others, sample H-76-11 was not white before coloring, so a picture of it before irradiation is added in the figure. For comparison, also picture of BH0.1 before irradiation is added. Pictures of the other samples before irradiation are not added, as they were all the same, white color as sample BH0.1.*

Sample H-11-S-3 has another, non-photochromic phase, nepheline, but its deep reflectance valley and strong purple color make it an interesting candidate for additional research. The reflectance valley

could be expected to be much smaller, as it seems to have much of the additional nepheline, while the other samples contain only hackmanite phase. However, the results show the opposite, so the synthesis procedure could be examined more. In order to achieve a more pure hackmanite without nepheline phase, the annealing could be repeated after remixing the sample with additional sodium bromide, as Radler stated in the original experiment.[51] By making a new sample with H-11-S-3 composition, and following the changes in composition and tenebrescent properties after each annealing-NaBr addition cycle, an alternative synthesis route could be examined and optimized.

Another very essential step in research concerning hackmanite glass structures is pellet formation. These experiments were done with powdery hackmanite, as more focus was put in the behavior of flux agents with hackmanite and higher synthesis temperatures often required for glass making. In order to better study the properties of hackmanite in actual glass-like material, it could be pressed into a pellet with some additional silica, as it was found to be a promising addition in Radler's research.[51] A pellet would reduce the amount of air pockets and ensure uniformity in melting. More research is thus needed, but the addition of boric oxide showed very promising results, giving optimistic signs in the aim of making hackmanite-containing glass. In addition to the topics mentioned, hot-pressing technique could provide the needed transparency of the pellet and should be investigated more.

3.6. Hackmanite synthesis by precipitation and reduction tests

Since solid state synthesis produced aggregated particles, precipitation synthesis was tested for obtaining separate crystallites. Hackmanite synthesized with precipitation from an aluminosilicate solution showed good results in the case of purity and crystallite size **(Table S2, Supporting Information)**, even though the reflectance valley was about 10 percentage points smaller than that of hackmanite H7.5 **(Figure 2B)**. The synthesized hackmanite showed quite exactly the same kind of diffraction patterns before and after reduction **(Figure 18A)**, indicating that there were no impurities present after the precipitation, and after the reduction process conducted in a furnace. The samples that were attempted to be reduced using $NaBH_4$, and additionally including formic acid, also have all the characteristic hackmanite peaks. However, the reduction didn't succeed with those samples, as only the sample reduced in a furnace has a reflectance valley **(Figure 18B)**.

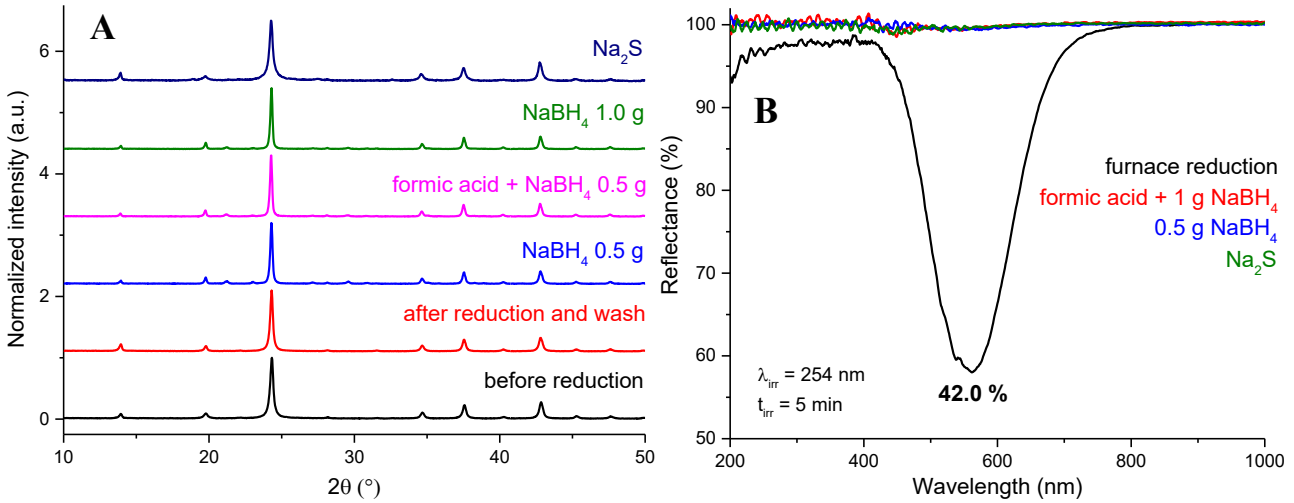

Figure 18. *XRD patterns* ***(A)*** *of hackmanite samples attempted to be reduced using different methods, and reflectance spectra* ***(B)*** *of samples reduced using those four different approaches: furnace, $NaBH_4$, formic acid together with $NaBH_4$ and Na_2S. All reflectance spectra are normalized to 100 % reflectance at 950 nm, and the depth of the single valley is included in the figure.*

The reduction of sulfate to sulfide is highly dependent on temperature and pH and typically requires a strong reducing agent, such as hydrogen gas or carbon. The concentration of sulfate and reducing agents in the solution significantly influences the reaction speed and completion. Higher temperatures cause the ions to collide more often, leading to higher reaction rate. When reducing sulfate, where sulfur is in a +6 oxidation state, to sulfide, where sulfur is in a –2 oxidation state, the sulfur often transforms into intermediate sulfur compounds before achieving complete reduction. Acidic conditions favor the formation of these reactive intermediates, shifting the reaction equilibrium towards the reduction process. Consequently, previous research on sulfate reduction has shown that temperatures over 200 °C, highly acidic conditions, and often hydrothermal conditions are required in order to achieve a high reduction rate.[58–61]

Reducing the SO_4^{2-} to S_2^{2-} using $NaBH_4$ did not thus succeed, which can be attributed to the insufficient reduction temperature. This is because the sulfate ion is very stable due to the sulfur's high positive oxidation state of +6, and thus a lot of energy is needed to break its bonds. In order to continue with the alternative reduction method, the limitation of the boiling point of water (100 °C) needs to be avoided by utilizing higher boiling point solvents, such as oleic acid, which has a boiling point of approximately 360 °C. Another factor to focus on is the reaction environment, as in the original publication[62] a hydrothermal method was conducted after the precipitation. An autoclave could be utilized in future experiments to explore if the reduction could be done in higher temperatures and pressures, even though the achieved temperatures would not be as high as when using furnaces. The results of these reduction experiments highlight the need for better experimental conditions to achieve the desired sulfate reduction within hackmanite. By exploring higher temperature solvents, implementing hydrothermal conditions via an autoclave, testing alternative

reducing agents, and systematically optimizing other reaction parameters, future research could potentially achieve sulfate reduction in hackmanite without using a furnace.

3.7. Optimization of reduction temperature

As a second way of decreasing the possibility for aggregation, changing the reduction temperature was investigated. The reflectance properties of hackmanite samples reduced at different temperatures follow a clear trend, where samples reduced at higher temperatures, from 700 °C to 850 °C, all exhibit significantly deeper reflectance valleys than those reduced at lower temperatures **(Figure 19)**. This outcome aligns with expectations, as effective sulfate reduction is essential for hackmanite's coloration process. At lower reduction temperatures, sulfate is not fully converted to sulfide, which directly limits the formation of color centers within the structure. As a result, samples reduced at lower temperatures have shallower reflectance valleys and less intense coloration.

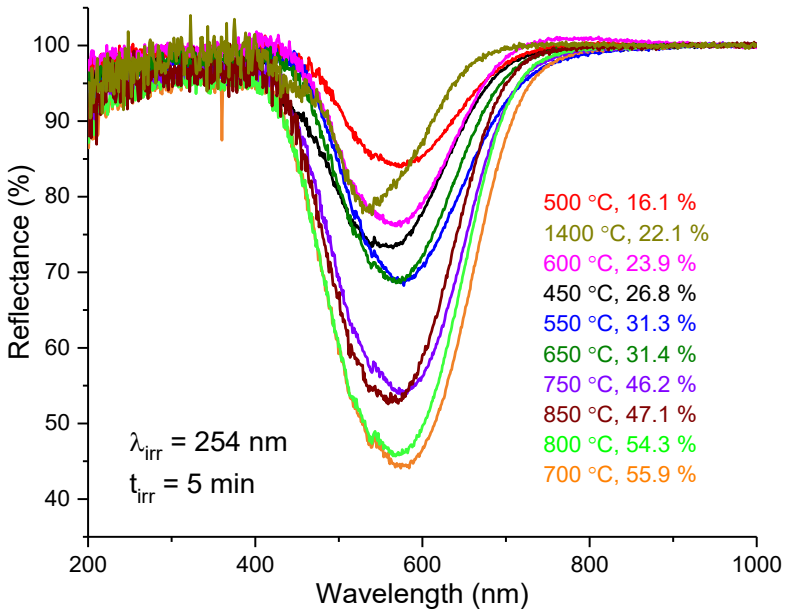

Figure 19. *Reflectance spectra of reduction temperature test hackmanites. All reflectance spectra are normalized to 100 % reflectance at 950 nm. The reduction temperature and depth of the reflectance valley are reported in the figure in the order of descending valley.*

Sample reduced at 1400 °C has a very small valley, regardless of the high reduction temperature. This is most likely due to loss of bromide in such high temperatures, leading to destabilization and breakage of the hackmanite structure. The XRF measurement confirms this – other hackmanite samples have 35–45 % of Br, while this sample reduced at 1400 °C has only 18 % **(Table S4, Supporting Information)**.

These differences in the valley depth can also be seen by eye from the color of the hackmanite after it was irradiated with 254 nm UV light for 5 minutes **(Figure 20)**. Hackmanite reduced at temperatures 650 °C and below have much smaller reflectance valleys and only a weak pastel purple

color. In contrast, samples reduced at above 700 °C, excluding the sample reduced at 1400 °C, have a very deep valley, leading to intense, clearly distinguishable purple color.

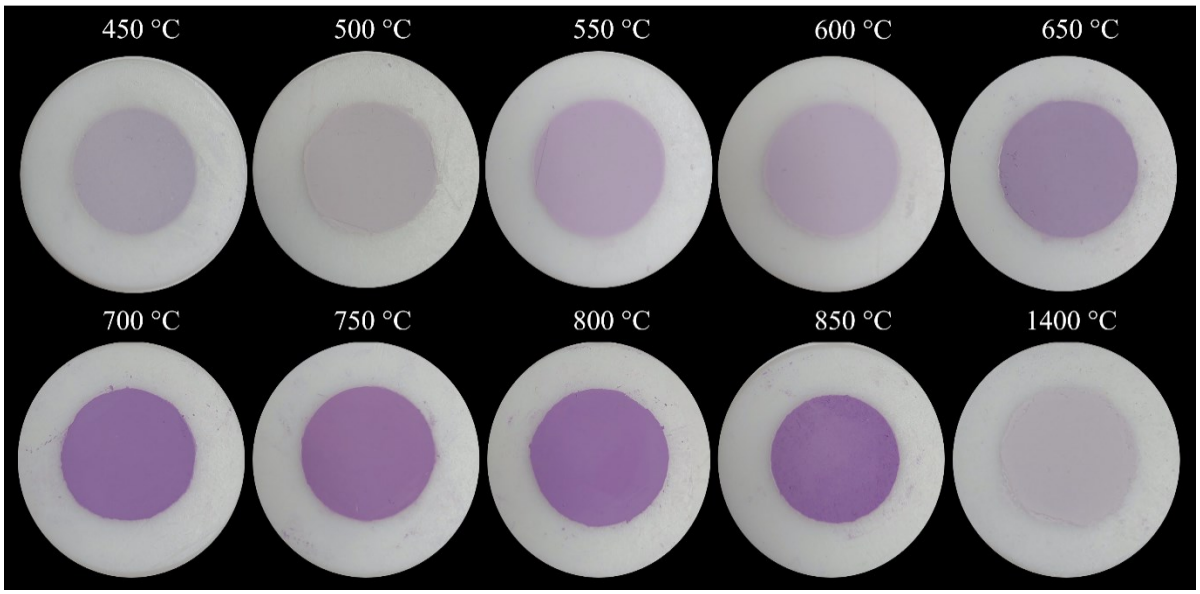

Figure 20. *Pictures of colored hackmanite samples. The pictures were taken after irradiating the samples for 5 minutes with 254 nm UV light, and the contrast of the pictures was adjusted to enhance the distinction between the colored material and the white sample holder. The used reduction temperature is added in the figure. As all the hackmanites exhibit the same white color before UV irradiation, no pictures before coloration were added.*

The findings of these experiments suggest that 700 °C to 850 °C represents an optimal reduction temperature range for hackmanite synthesis, high enough to provide effective sulfate reduction. At these temperatures, hackmanite achieves maximum color center formation without significant bromide volatilization. Avoiding excessive temperatures, such as 1400 °C, is crucial, as the bromide loss observed at such levels leads to a notable decline in photochromic performance. In the future, by exploring the temperatures within the range of 700 °C to 850 °C the temperature could be optimized more to find the specific temperature that maximizes color center formation while minimizing bromide and overall tenebrescence loss. The reduction duration at these temperatures could also be optimized to assess whether extended reduction times could improve sulfate conversion without reducing the color-change efficiency. These findings provide a foundation for further optimization of reduction temperatures in hackmanite synthesis, underscoring the critical balance between temperature control and chemical stability to achieve optimal photochromic properties.

3.8. Acrylic hackmanite disks

As the final part of this work, the material with optimized photochromism intensity and crystallite size was tested for incorporation into a transparent organic polymer. This would avoid the high temperatures needed for doping into glass. The biggest goal in this experiment was to maintain the photochromic feature of hackmanite even when mixed with Technovit, and it succeeded. Main reason of concern was if Technovit would block the wavelengths needed to excite the color-change in

hackmanite. However, as the hackmanite mass percentage was as high as 10 % in all the samples, deeper color could have been expected to form. The depths of the reflectance valleys are ~21–27 % **(Figure 21A)**, similar to measured valleys of films with 0.7–1.7 m-% of hackmanite **(Figure 4 and Figure 8A)**. The disks are much thicker compared to the films, so the results are not fully comparable. Still, due to the very much higher hackmanite content, the reflectance valley would be expected to be deeper and the color of the disks much more intensive. Now, all the samples were only pale purple **(Figure 21B)**. Disk 3, which was made thinner, has very rough edges, whereas the thicker disks 1 (~3.67 mm) and disk 2 (~1.95 mm) have smoother and more even surface. This inconsistency in thickness of disk 3, which can also be seen with naked eye, is large throughout the material, as in one edge it is 2.06 mm thick and 1.41 mm in another.

In addition to the weak coloration, the samples appeared very matte and opaque, which then made the light transmittance quite nonexistent. As the samples were prepared following the instructions on how the Technovit samples should be made in order to achieve transparency – in high pressure and very quickly due to the rapid curing time – this was unexpected. However, as in this experiment the PressurePot of the manufacturer, designed for this specific material, was not available, some minor differences in the synthesis might have caused the opacity.

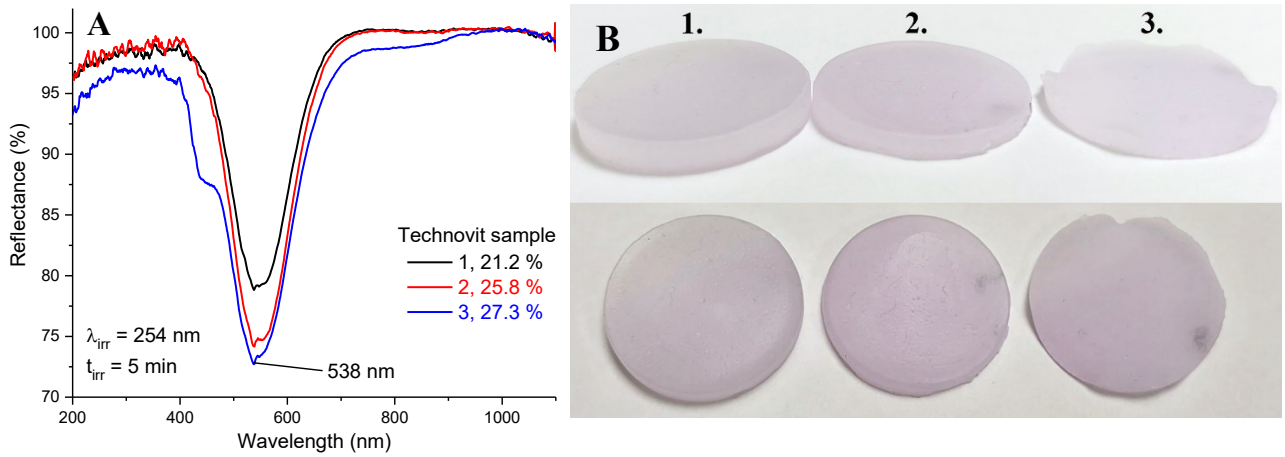

Figure 21. *Reflectance spectra* ***(A)*** *and pictures of the three colored acrylic disks* ***(B)****. All reflectance spectra are normalized to 100 % reflectance at 1000 nm, and the depth of the reflectance valleys at 538 nm are reported in the figure. The pictures were taken after irradiating the samples for 5 minutes with 254 nm UV light, and the brightness is adjusted to enhance the distinction between the colored material and the white paper.*

The disks were not analyzed further, nor more were made due to weak transmittance and coloration. In the future, the combination of hackmanite with other polymers could be researched further, as the main feature of hackmanite – tenebrescence – remains in the materials, even though the coloration should be enhanced. The use of Technovit could also be explored more. If PressurePot was available, the curing could be done there to possibly enhance especially the transmittance. The surfaces of the disks could also be polished in order to see if the opacity is present within the whole disk, or just the surfaces.

4. Conclusions

The initial goal of this study was to first synthesize hackmanite films and study their characteristics, and then move on to further experimentation of hackmanite lenses instead of films, as they are more suitable for eyewear application. However, challenges faced in another work carried out at the same time within the research group in combining hackmanite with glass shifted the focus toward a broader investigation of its photochromic properties. There is no published research or additional documentation available on this work, but the extensive research showed limited potential in incorporation of hackmanite within glass, so the incorporation was not further explored in this work either, and the focus was kept on optimization of hackmanite's characteristics and synthesis process.

The sunlight contains a large amount of UV radiation especially within the UV-A range (320–400 nm) **(Figure 6A)**, which is why the optimal activation wavelength for materials used in photochromic glasses would be in that wavelength range. This would make the photochromic material respond more effectively to the typical outdoor conditions, enabling quick coloring. The activation wavelength cannot either be too long, near the visible light range, as then it could darken also indoors. The samples prepared in this study obtain the deepest color under 254 nm irradiation, which is in the UV-C range. However, UV-C irradiation is primarily blocked by the Earth ozone layer, meaning that to obtain a deep color outdoors and to show more potential in the field of photochromic eyewear, the optimal activation wavelength of hackmanite should be increased and activation energy thus decreased. This has already been done by Norrbo et al.[3] by substitution of Na with K or Rb. Even though the highest color intensity was still achieved with UV-C wavelengths, significant shift towards longer excitation wavelengths was achieved. This result underlines the great potential of hackmanite in commercial applications, as long as more research is being done.

This study investigated various synthesis techniques, material compositions, and processing parameters to enhance the photochromic properties of hackmanite, focusing on the potential use of hackmanite in photochromic eyewear. The experiments focused on optimizing crystal size, reduction conditions, film preparation and aggregation control. The hackmanite samples synthesized showed good photochromic properties, with the grinding set providing information about the relationship between crystal size and reflectance valley depth. The findings indicate that smaller crystal sizes generally promote better light absorption, minimizing scattering and increasing transparency in film applications. However, samples ground for longer showed reduced UV absorption, potentially due to structural damage during the too long grinding process. Hackmanite H7.5 emerged as the most promising candidate, balancing small crystal size with high absorptance, making it suitable for further experiments in film production. For eyewear applications, hackmanite's longer fading time presents a challenge compared to commercial products, which typically fade within 5–10 minutes. However,

the fast coloration rate of hackmanite underlines its potential in UV sensors, as in them, transparency is not a needed feature.

The exploration of boron additions demonstrated that boron-containing hackmanites showed better UV absorption than those without boron, but excessive boron led to the formation of secondary phases, such as nepheline, and diminished photochromic response. The optimal boron content was determined to be around 0.1 g per sample, emphasizing the importance of precise control over flux agent concentrations.

Successful reduction is critical in hackmanite synthesis, as the sulfate-to-sulfide conversion is a process necessary for hackmanite's photochromic mechanism. The best photochromic performance was achieved with reduction temperatures between 700 °C and 850 °C, as these temperatures seem to maximize color center formation. Samples reduced at lower temperatures had less intense coloration due to incomplete sulfate reduction, while the sample exposed to temperature 1400 °C exhibited structural degradation, particularly through bromide loss. These findings highlight the need for careful temperature control. Alternative reduction methods using $NaBH_4$ did not show promising results, as the sulfate reduction requires high temperatures which these experiments did not have. In the future, higher temperature solvents or hydrothermal reduction using an autoclave could be researched more.

The main hindrance in the study of the needed properties for hackmanite to be used in photochromic eyewear was the absence of a base material that could actually be used in them. For lack of better material, elastomer film was used, but it does not accurately represent the commercially used base materials, such as glass or transparent polymer matrices. The hackmanite film sets demonstrated that higher hackmanite mass percentages led to deeper reflectance valleys and more intense coloration, but also to increased opacity and light scattering. The aggregation and clumping of hackmanite particles could not be reduced with additives, as using them resulted in weakened UV absorption. This highlights the need for alternative dispersion strategies to achieve a more transparent material.

Finally, hackmanite was incorporated into Technovit acrylic resin to create a thicker, more transparent lens material suitable for applications in eyewear and optical devices. However, the color intensity of these films was rather weak compared to hackmanite–elastomer films, despite significantly higher hackmanite content. The Technovit disks appeared opaque and matte, with minimal transmittance. These results suggest that future studies should explore other polymer matrices compatible with hackmanite.

Additionally, alternative synthesis routes such as sol-gel or hot-press techniques could be explored more to prepare more transparent materials. Sol-gel synthesis, which is used in the making of glass materials, would be a promising alternative, as it requires much lower synthesis temperatures compared to the traditional glass-making temperatures. It has already been used in the making of photochromic glass[63], showing promising results under just 350 °C heating. However, as previously stated, the synthesis of hackmanite glass material did not work, even in the case of sol-gel synthesis. This could be due to an unknown reaction with hackmanite and tetraethoxysilane (TEOS), which is used the most in sol-gel syntheses. This unwanted result could be due to undesirable interaction between the developing silica network and hackmanite, the very long sol-to-gel drying process, or the annealing done to finalize the condensation process. An alternative method in synthesis of photochromic glass would be the traditionally used melt-quenching method, but it requires temperatures of over 1300 °C, which are too high for hackmanite, as could be seen from the hackmanite reduced at 1200 °C.[26].

This study offered the basis of the research concerning the use of hackmanite in photochromic eyewear. The results show hackmanite's potential for photochromic applications, even though achieving the desired color intensity and transparency, and finding the suitable, transparent base material requires further research. The wavelength that causes the strongest color change of hackmanite by generating the F-centers was 254 nm with these samples. The samples did show some coloration under irradiation of 302 nm UV lamp, but as the main focus was to achieve a very deep color within the studied material, the measurements were done only using the 254 nm UV lamp. In further experiments, also 302 nm and 365 nm UV lamps should be used to better see the behavior of hackmanite within the synthesized elastomer films and in other experiments, such as when adding boron.

References

1. Armstrong, J. A., Weller M.T. Structural observation of photochromism. *Chem Commun*. **2006**, *10*, 1094–1096. doi:10.1039/b517715d

2. Lawrynowicz, A., Vuori, S., Palo, E., Winther, M., Lastusaari, M., Miettunen, K. Transforming fabrics into UV-sensing wearables: A photochromic hackmanite coating for repeatable detection. *Chem Eng J*. **2024**, *494*. doi:10.1016/j.cej.2024.153069

3. Norrbo, I., Curutchet, A., Kuusisto, A., Mäkelä, J., Laukkanen, P., Paturi, P., Laihinen, T., Sinkkonen, J., Wetterskog, E., Mamedov, F., Le Bahers, T., Lastusaari, M. Solar UV index and UV dose determination with photochromic hackmanites: From the assessment of the fundamental properties to the device. *Mater Horiz*. **2018**, *5*, 569-576. doi:10.1039/c8mh00308d

4. Vuori, S., Colinet, P., Lehtiö, J.P., Lemiere, A., Norrbo, I., Granström, M., Konu, J., Ågren, G., Laukkanen, P., Petit, L., Airaksinen, A., van Goethem, L., Le Bahers, T., Lastusaari, M. Reusable radiochromic hackmanite with gamma exposure memory. *Mater Horiz*. **2022**, *9*, 2773-2784. doi:10.1039/d2mh00593j

5. Badour, Y., Danto, S., Albakour, S., Mornet, S., Penin, N., Hirsch, L., Gaudon, M. Low-cost WO_3 nanoparticles / PVA smart photochromic glass windows for sustainable building energy savings. *Sol Energ Mat Sol C*. **2023**, *255*., 112291–112301. doi:10.1016/j.solmat.2023.112291

6. Vuori, S., Colinet, P., Norrbo, I., Steininger, R., Saarinen, T., Palonen, H., Paturi, P., Rodrigues, L.C.V., Göttlicher, J., Le Bahers, T., Lastusaari, M. Detection of X-Ray Doses with Color-Changing Hackmanites: Mechanism and Application. *Adv Opt Mater*. **2021**, *9*, 2100762. doi:10.1002/adom.202100762

7. Raymo, F. M., Tomasulo, M. Optical processing with photochromic switches. *Chem Eur J*. **2006**, *12*, 3186-3193. doi:10.1002/chem.200501178

8. Caurant, D., Gourier, D., Prassas, M. Electron-paramagnetic-resonance study of silver halide photochromic glasses: Darkening mechanism. *J Appl Phys*. **1992**, *71*, 1081-1090. doi:10.1063/1.351400

9. Arminstead, W. H., Stookey, S. D. Photochromic Silicate Glasses Sensitized by Silver Halides. *Science (1979)*. **1964**, *144*, 150-154. doi:10.1126/science.144.3615.150

10. Zhao, H., Cun, Y., Bai, X., Xiao, D., Qiu, J., Song, Z., Liao, J., Yang, Z. Entirely Reversible Photochromic Glass with High Coloration and Luminescence Contrast for 3D Optical Storage. *ACS Energy Lett*. **2022**, *7*, 2060-2069. doi:10.1021/acsenergylett.2c00574

11. Agamah, C., Vuori, S., Colinet, P., Norrbo, I., de Carvalho, J., Nakamura, L., Lindblom, J., van Goethem, L., Emmermann, A., Saarinen, T., Laihinen, T., Laakkonen, E., Linden, J., Konu, J., Vrielinck, H., Van der Heggen, D., Smet, P.F., Le Bahers, T., Lastusaari, M. Hackmanite-the natural glow-in-the-dark material. *Chem Mater*. **2020**, *32*, 8895-8905. doi:10.1021/acs.chemmater.0c02554

12. Curutchet, A., Le Bahers, T. Modeling the Photochromism of S-Doped Sodalites Using DFT, TD-DFT, and SAC-CI Methods. *Inorg Chem*. **2017**, *56*, 414-423. doi:10.1021/acs.inorgchem.6b02323

13. Byron, H. C., Swain, C., Paturi, P., Coliner, P., Rullan, R., Halava, V., Le Bahers, T., Lastusaari, M. Highly Tuneable Photochromic Sodalites for Dosimetry, Security Marking and Imaging. *Adv Funct Mater*. **2023**, *33*, 6264-6285. doi:10.1002/adfm.202303398

14. Bianco, A., Bertarelli, C., Dassa, G., Toso, G., Zerbi, G. Realization of photochromic-polymeric films for optical applications. In: *CIMTEC 2008 - Proceedings of the 3rd International Conference on Smart Materials, Structures and Systems - Smart Optics*. **2008**, *55*, 1-6. doi:10.4028/www.scientific.net/AST.55.1

15. Yun, C., You, J., Kim, J., Huh, J., Kim, E. Photochromic fluorescence switching from diarylethenes and its applications. *J Photoch Photobio C*. **2009**, *10*, 111-129. doi:10.1016/j.jphotochemrev.2009.05.002

16. Raymo, F. M., Tomasulo, M. Fluorescence modulation with photochromic switches. *J Phys Chem A*. **2005**, *109*, 7343-7352. doi:10.1021/jp052440o

17. Song, C., Guo, Q., Liu, Y., Rao, Y., Liao, L. Photochromism, UV-Vis, Vibrational and Fluorescence Spectroscopy of Differently Colored Hackmanite. *Crystals*. **2023**, *13*, 1607-1618. doi:10.3390/cryst13111607

18. Ru, Y., Shi, Z., Zhang, J., Wang, J., Chen, B., Huang, R., Liu, G., Yu, T. Recent progress of photochromic materials towards photocontrollable devices. *Mater Chemi Front*. **2021**, *5*, 7737-7758. doi:10.1039/d1qm00790d

19. Wang, L., Li, Q. Photochromism into nanosystems: Towards lighting up the future nanoworld. *Chem Soc Rev*. **2018**, *47*, 1044-1097. doi:10.1039/c7cs00630f

20. Klajn R. Spiropyran-based dynamic materials. *Chem Soc Rev*. **2014**, *43*, 148-184. doi:10.1039/c3cs60181a

21. Pardo R, Zayat M, Levy D. Photochromic organic-inorganic hybrid materials. *Chem Soc Rev*. **2011**, *40*, 672-687. doi:10.1039/c0cs00065e

22. Julià-López, A., Ruiz-Molina, D., Hernando, J., Roscini, C. Solid Materials with Tunable Reverse Photochromism. *ACS Appl Mater Inter*. **2019**, *11*, 11884-11892. doi:10.1021/acsami.8b22335

23. Merino, E., Ribagorda, M. Control over molecular motion using the cis-trans photoisomerization of the azo group. *Beilstein J Org Chem*. **2012**, *8*, 1071-1090. doi:10.3762/bjoc.8.119

24. Kayani, A.B.A., Kuriakose, S., Monshipouri, M., Khalid, F.A., Walia, S., Sriram, S., Bhaskaran, M. UV Photochromism in Transition Metal Oxides and Hybrid Materials. *Small*. **2021**, *17*, 2100621. doi:10.1002/smll.202100621

25. Lu, H., Zheng, Z., Li, Z. J., Bao, H., Guo, X., Guo, X., Lin, J., Qian, Y., Wang, J.Q. Achieving UV and X-ray dual photochromism in a metal-organic hybrid via structural modulation. *ACS Appl Mater Interfaces*. **2021**, *13*, 2745-2752. doi:10.1021/acsami.0c20036

26. Zhu, X., Huang, A., Zhao, H., Liu, Y., Cun, Y., Song, Z., Qiu, J., Tatiana, C., Liao, J., Yang, Z. Defects-Induced Photochromism and Luminescent Modulation Based on Lanthanides-Doped Cadmium Glass Toward Optical Storage Applications. *Laser Photonics Rev*. **2024**, *18*, 2301326. doi:10.1002/lpor.202301326

27. Norrbo, I., Hyppänen, I., Lastusaari, M. Up-conversion luminescence – A new property in tenebrescent and persistent luminescent hackmanites. *J Lumin*. **2017**, *191*, 28-34. doi:10.1016/j.jlumin.2017.02.046

28. Norrbo, I., Gluchowski, P., Paturi, P., Sinkkonen, J., Lastusaari, M. Persistent Luminescence of Tenebrescent $Na_8Al_6Si_6O_{24}(Cl,S)_2$: Multifunctional Optical Markers. *Inorg Chem*. **2015**, *54*, 7717-7724. doi:10.1021/acs.inorgchem.5b00568

29. Norrbo, I., Carvalho, J. M., Laukkanen, P., Mäkelä, J., Mamedov, F., Peurla, M., Helminen, H., Pihlasalo, S., Härmä, H., Sinkkonen, J., Lastusaari, M. Lanthanide and Heavy Metal Free Long White Persistent Luminescence from Ti Doped Li–Hackmanite: A Versatile, Low-Cost Material. *Adv Funct Mater*. **2017**, *27*, 1606547. doi:10.1002/adfm.201606547

30. Byron, H., Norrbo, I., Lastusaari, M. A zeolite-free synthesis of luminescent and photochromic hackmanites. *J Alloy Compd*. **2021**, *872*, 159671. doi:10.1016/j.jallcom.2021.159671

31. Byron, H., Kreivilä, T., Colinet, P., Le Bahers, T., Lastusaari, M. New shades of photochromism - yellow sodalites for the detection of blue light. *J Mater Chem C*. **2023**, *11*, 3360–3374. doi:10.1039/d3tc00116d

32. Zahoransky, T., Friis, H., Marks, M. A. W. Luminescence and tenebrescence of natural sodalites: a chemical and structural study. *Phys Chem Miner*. **2016**, *43*, 459-480. doi:10.1007/s00269-016-0810-0

33. Norrbo, I., Gluchowski, P., Hyppänen, I., Laihinen, T., Laukkanen, P., Mäkelä, J., Mamedov, F., Santos, H.S., Sinkkonen, J., Tuomisto, M., Viinikanoja, A., Lastusaari, M. Mechanisms of Tenebrescence and Persistent Luminescence in Synthetic Hackmanite $Na_8Al_6Si_6O_{24}(Cl,S)_2$. *ACS Appl Mater Inter*. **2016**, *8*, 11592-11602. doi:10.1021/acsami.6b01959

34. Colinet, P., Byron, H., Vuori, S., Lehtiö, J-P., Laukkanen, P., van Goethem, L., Lastusaari, M., Le Bahers, T. The structural origin of the efficient photochromism in natural minerals. *P Natl Acad Sci USA*. **2022**, *119*, 1-7. doi:10.1073/pnas.2202487119

35. International Mineralogy Association. List of Minerals. http://cnmnc.units.it/imalist.htm. Accessed 6.6.2024.

36. Vuori, S. Reversible photochromism of synthetic hackmanites in radiation detection and quantification. *University of Turku*. **2023**. [Online]

37. Goudjil, K. Photochromic Ultraviolet Protective Shield. *Inorg Opt Mater II*. **2000**, *4102*, 289-298. doi:10.1117/12.405295

38. El-Zaiat, S.Y., Medhat, M., Omar, M.F., Shirif M.A. Effect of UV exposure on photochromic glasses doped with transition metal oxides. *Opt Commun*. **2016**, *370*, 176-182. doi:10.1016/j.optcom.2016.03.010

39. Moukova, A., Malina, L., Kolarova, H., Bajgar, R. Hyperoside as a UV Photoprotective or Photostimulating Compound—Evaluation of the Effect of UV Radiation with Selected UV-Absorbing Organic Compounds on Skin Cells. *Int J Mol Sci*. **2023**, *24*, 9910. doi:10.3390/ijms24129910

40. Fang, W., Sairanen, E., Vuori, S., Rissanen, M., Norrbo, I., Lastusaari, M., Sixta, H. UV-Sensing Cellulose Fibers Manufactured by Direct Incorporation of Photochromic Minerals. *ACS Sustain Chem Eng*. **2021**, *9*, 16338-16346. doi:10.1021/acssuschemeng.

41. International Energy Agency (IEA). *Transition to Sustainable Buildings: Strategies and Opportunities to 2050*. 1st edition. International Energy Agency, **2013**, 117-127.

42. Allouhi, A., El Fouih, Y., Kousksou, T., Jamil, A., Zeraouli, Y., Mourad, Y. Energy consumption and efficiency in buildings: Current status and future trends. *J Clean Prod*. **2015**, *109,* 118-130. doi:10.1016/j.jclepro.2015.05.139

43. Ahmadi, K., Khakpoor, A.A. Oxide glasses doped with silver nanoparticles: properties and technologies. *Int Mat Phys J*. **2013**, *1*, 40-46. doi:10.1080/10587250008023814

44. Kotb, O.M, El Ghazaly, M., Mohamed, A., Ibrahim, M.A. Investigation on response of ophthalmic photochromic TRANSITIONS SIGNATURE® VII lens to ultraviolet radiation. *Optik (Stuttg)*. **2022**, *268*, 169772-169779. doi:10.1016/j.ijleo.2022.169772

45. Van Gemert, B. Commercialization of plastic photochromic lenses: a tribute to John Crano. *Mol Cryst Liq Crys A*. **2000**, *344*, 57-62. doi:10.1080/10587250008023814

46. Essilor. "Essilor Transitions Lenses." Accessed October, 2024. https://www.essilor.com.

47. Zeiss. "PhotoFusion Lenses." Accessed October, 2024. https://www.zeiss.com.

48. Younger Optics. "Drivewear Lenses." Accessed October, 2024. https://www.youngeroptics.com.

49. Hoya Vision. "Sensity Photochromic Lenses." Accessed October, 2024. https://www.hoyavision.com.

50. Transitions Optical. "Transitions Signature Lenses." Accessed October, 2024. https://www.transitions.com.

51. Radler, R. Inorganic phototropic materials for high density computer memories. *AD-407796*. Published online **1963**. Accessed February 15, 2024. https://apps.dtic.mil/sti/citations/AD0407796

52. Hund F. Nitrit-, Cyanid- und Rhodanid-Sodalith. *Anorg Allg Chem*. **1984**, *511*, 225-230.

53. Eppig, T., Speck, A., Gillner, M., Nagengast, D., Langenbucher, A. Photochromic dynamics of ophthalmic lenses. *Appl Optics*. **2012**, *51*, 133-138. doi:10.1364/AO.51.000133

54. National Renewable Energy Laboratory. Reference Air Mass 1.5 Spectra. *U.S. Department of Energy.* Retrieved from https://www.nrel.gov/grid/solar-resource/spectra-am1.5.html.

55. King-Smith, P.E., Kranda, K. Photopic adaptation in the red-green spectral range. *Vision res*. **1980**, *21*, 565-572.

56. CIE spectral luminous efficiency for scotopic and photopic vision. *International Commission on Illumination (CIE), Vienna, Austria*.

57. Valaulikar, B.S, Manohar, C. The Mechanism of Clouding in Triton X-100: The Effect of Additives. *J Colloid Interface Sci*. **1985**, *108*, 403-406.

58. Spirakis, C.S. The possible role of sulfate-reduction kinetics in the formation of hydrothermal uranium deposits. *Economic Geology*. **1981**, *76*, 2236-2239. doi:10.2113/GSECONGEO.76.8.2236

59. Ohmoto, H., Lasaga, A.C. Kinetics of Reaetions between Aqueous Sulfates and Sulfides in Hydrothermal Systems. *Geochim Cosmochim AC*. **1982**, 46, 1727-1745.

60. Kiyosu', Y., Roy, H. Thermochemical Reduction by Acetic Acid in and Sulfur Isotopic Behavior of Sulfate the Presence of Native Sulfur. *Geochem J.* **1993**, *27*, 49-57. doi:10.2343/geochemj.27.49

61. Zhang, T., Amrani, A., Ellis, G.S., Ma, Q., Tang, Y. Experimental investigation on thermochemical sulfate reduction by H_2S initiation. *Geochim Cosmochim Acta*. **2008**, *72*, 3518-3530. doi:10.1016/j.gca.2008.04.036

62. Weller, M.T., Dodd, S.M., Jiang, M.R.M. *Synthesis, Structure and Ionic Conductivity in Nitrite Sodalites*. J Mater Chem. **1991**, *1*, 11-15.

63. Al-Qahtani, S.D., Alzahrani, S.O., Snari, R.M., Al-Ahmed, Z.A., Alkhamis, K., Alhasani, M., El-Metwaly, N.M. Preparation of photoluminescent and photochromic smart glass window

using sol-gel technique and lanthanides-activated aluminate phosphor. *Ceram Int*. **2022**, *48*, 17489-17498. doi:10.1016/j.ceramint.2022.03.013

SUPPORTING INFORMATION

Table S1. *Used furnaces in different syntheses.*

Sample	Lenton	Carbolite Gero	Lindberg Blue/M	Big Elite
H0		x		
H2.5		x		
H5		x		
H7.5		x		
H10		x		
H12.5		x		
BH0.05		x (reduction)		x
BH0.1		x (reduction)		x
BH0.14		x		
BH0.17		x		
H-11-S-3	x			
H-76-11	x			
precipitated hackmanite			x (reduction)	
hackmanite for temperature set tests		x		
450 °C			x (reduction)	
500 °C			x (reduction)	
550 °C			x (reduction)	
600 °C			x (reduction)	
650 °C			x (reduction)	
700 °C			x (reduction)	
750 °C			x (reduction)	
800 °C			x (reduction)	
850 °C			x (reduction)	
1400 °C	x (reduction)			

Table S2. *Crystallite sizes calculated from the hackmanite peak in XRD graphs using the Scherrer equation. In addition to crystalline size, 2θ, β and $\beta_{instr.}$ values are included. $\beta_{instr.}$ values are reported with three decimals due to smaller values.*

Batch	Hackmanite	2θ (°)	β (°)	$\beta_{instr.}$ (°)	Crystalline size (nm)
Grinding set	H2.5	24.53	0.14	0.089	75.34
	H5.0	24.49	0.15	0.089	70.34
	H7.5	24.56	0.17	0.089	55.72
	H10	24.42	0.14	0.089	71.92
	H12.5	24.43	0.15	0.089	68.84
	H0	24.58	0.15	0.089	66.72
Boron sets	BH0.05	24.27	0.14	0.077	66.82
	BH0.1	24.31	0.14	0.077	71.02
	BH0.14	24.34	0.30	0.077	27.74
	BH0.17	24.33	0.23	0.077	37.51
	H-11-S-3	24.31	0.14	0.077	68.85
	H-76-11	24.29	0.13	0.077	81.56
	Precipitated hackmanite	24.31	0.22	0.089	39.80

Table S3. *The reflectance measurement setup used in each measurement.*

Sample set	optical fiber	integrating sphere
Grinding set	**X**	
1st film set	**X**	
2nd film set	**X**	
Aggregation control films	**X**	
Boron set hackmanites		**X**
Precipitated hackmanites		**X**
Reduction test set		**X**
Reduction temperature test set		**X**
Acrylic disks	**X**	

Table S4. *XRF results of boron set, reduction test set, and reduction temperature set samples. Unfortunately, XRF results of grinding set samples are not available.*

	Sample	Al	Si	S	Cl	K	Br
Boron set	BH0.05	21.44	32.76	0.37	4.57	4.00	36.86
	BH0.1	22.63	34.71	0.49	2.15	2.63	37.39
	BH0.14	23.92	35.90	1.70	3.87	3.35	31.26
	BH0.17	22.87	34.30	1.38	2.53	4.59	34.32
	H-11-S-3	27.92	43.57	0.18	0.85	0.66	26.82
	H-76-11	20.94	33.51	0.43	0.87	0.69	43.56
		Al	Si	S	Cl	K	Br
reduction test set	Reduced in furnace	23.47	34.27	0.81	0.61	0.07	40.76
	$NaBH_4$ 0.5 g	22.67	34.82	0.84	0.45	3.56	37.65
	$NaBH_4$ 0.5 g + acid	24.55	34.44	0.84	0.48	2.28	37.42
	$NaBH_4$ 1g + acid	28.80	48.92	6.76	0.56	-	14.97
	Na_2S	25.37	36.53	2.80	0.52	0.09	34.69
		Al	Si	S	Cl	K	Br
Reduction temperature set	450 °C	19.98	32.39	0.77	0.69	0.55	45.62
	500 °C	22.09	30.73	0.69	0.97	2.58	42.94
	550 °C	21.42	33.21	0.78	0.56	1.63	42.39
	600 °C	21.11	33.48	0.42	0.57	0.66	43.76
	650 °C	22.05	34.64	0.74	0.85	0.97	40.75
	700 °C	23.37	36.39	0.87	0.40	0.79	38.18
	750 °C	26.05	36.28	1.14	0.65	0.51	35.36
	800 °C	21.05	33.89	0.60	0.75	0.63	43.07
	850 °C	21.80	31.67	0.56	0.61	0.55	44.80
	1400 °C	56.67	23.15	0.19	0.63	0.93	18.43